DISCLAIMER:

This document does not meet the
current format guidelines of
the Graduate School at
The University of Texas at Austin.

It has been published for
informational use only.

A SUPERCONDUCTING GRAVIMETER FOR EVALUATION OF GROUNDWATER CHANGES IN THE FIELD

by

Hongqiu Wu, B.S.; M.S.

Thesis

Presented to the Faculty of the Graduate School of

The University of Texas at Austin

in Partial Fulfillment

of the Requirements

for the Degree of

Master of Science in Geological Sciences

The University of Texas at Austin

December, 2011

Abstract

A superconducting gravimeter for evaluation of groundwater changes in the field

Hongqiu Wu, MSGeoSci
The University of Texas at Austin, 2011

Supervisor: Clark R. Wilson

The Superconducting Gravimeter (SG) is an extremely sensitive instrument that measures relative changes in gravity. It is based on the movement of a superconducting sphere levitated in a magnetic field created by current in superconducting coils. It is capable of detecting gravity variations as small as 10^{-11} ms^{-2}. Because early production SG's lost helium at a steady rate, a large capacity dewar was required for reasonable periods of uninterrupted operation. In the late 1990's, Sumitomo Heavy Industries (SHI) developed a compact refrigeration system able to achieve liquid helium temperatures near 4K. It eliminates helium loss and allows a much smaller dewar to provide long intervals of continuous operation. These technical advances led us to develop an SG configured as a transportable field instrument. The goals were: 1) to package the entire SG system in two containers; 2) to test transport feasibility while the sensor remained in a superconducting levitated state; 3) to verify operability in field conditions; and 4) to determine the value of a transportable SG in groundwater and aquifer studies. We integrated the SG with a full weather station (measuring barometric pressure, rainfall, soil moisture etc.) and a geodetic GPS receiver (measuring vertical movement and atmospheric water vapor). All components were contained within enclosures constructed from angle and sheet aluminum. Each has dimensions ~1.5 x 0.8 x 1 m, total mass ~250 kg (including equipment) and can be transported easily by a medium truck while the sensor remained in a superconducting levitated state.

Temporal gravity variations measured by the SG include solid Earth tides, pole-tide, atmospheric pressure effect, ocean loading effect, and terrestrial water storage variations. Most of these can be well modeled, except the last term. We developed a standard procedure for SG data processing. The first field deployment of the SG system was for the study of the Edwards aquifer, a Karst aquifer system that provides water resources in Central Texas, and was operated by a monitoring well equipped with transducer to measure water level changes. The residual gravity changes measured by the SG were only sensitive to the water storage changes underground. With well level measurements, it can be used to estimate aquifer's specific yield.

Table of Contents

List of Tables

List of Figures

Chapter 1: Introduction

The Superconducting Gravimeter (SG) is the most sensitive instrument to measure relative changes in gravity (Neumeyer et. al. 2006). It was invented by John Goodkind and William Prothero at the University of California (Prothero and Goodkind 1968) and currently is manufactured by the GWR Instruments company at San Diego, California. The SG sensor consists of a spherical proof mass, levitated in magnetic fields created by electric currents in a pair of superconducting coils. When gravity changes, the sphere moves from its null position. The movement is sensed by capacitance plates surrounding the sphere and electric currents are applied through feedback coil to generate forces drawing the sphere back. The voltage is measured and calibrated into relative changes in gravity. According to manufacture's specification, the SG is capable of detecting gravity changes as small as 10^{-11} ms^{-2} (or 0.001 μGal). That is one part in one hundred billion of standard Earth gravity. At present, there are several dozens SG's operated over the world. A global network was set up under the Global Geodynamics Project (GGP) to compile significant data for a range of disciplines concerned with Earth's gravity, tides, environment, and geodetics (Crossley et al 1999). Even hydrologist and volcanologist can benefit from the data, by directly measuring mass changes underground caused by groundwater or magma changes.

Because early production SG lost helium at a steady rate, a large capacity dewar was required for reasonable periods of uninterrupted operation. In the late 1990's, Sumitomo Heavy Industries (SHI) developed a compact refrigeration system able to achieve liquid helium temperatures near 4K. It eliminates helium loss and allows a much smaller dewar to provide long intervals of continuous operation. When field replenishment of the helium bath is required (for example, after transporting the

instrument without the SHI refrigerator in operation), bottled helium gas can be liquefied at the instrument site. These technical advances led us to develop an SG configured as a transportable field instrument. The goals were to package the entire SG system in two containers, to test transport feasibility while the sensor remained in a superconducting levitated state, to verify operability in field conditions, and to determine the value of a transportable SG in groundwater and aquifer studies.

Generally, Earth's gravity is the sum of its own mass attraction, centrifugal force due to rotation, and tidal forces from the sun, moon and other planets. Earth's gravity varies over its surface, which reflects mass distribution including atmosphere, and water mass on and below Earth's surface. At one specific point on the surface, Earth's gravity also changes with time. The temporal Earth gravity changes consists of solid Earth tide, atmospheric pressure effect, oceanic loading effect, pole-tide effect, and terrestrial water storage variations. Their orders are shown in Table 1.1. Among them, solid Earth tides account for about 90% of gravity changes. The ocean loading effect depends on coast conditions and observation point's distance to the coast. Most tidal and other gravity effects can be well modeled, except for the effect of terrestrial water storage variation. Earth's gravity can be measured by satellites in space or gravimeters on the ground. For example, GRACE, launched in 2002, is an ongoing space mission to map Earth's gravity field by measuring changes in distance between two satellites. Its accuracy on surface gravity is about 0.9 μGal (Wahr et al 2004, 2006), but its spatial resolution is no better than a few hundred km.

Measurement of gravity at Earth surface by gravimeters has been undertaken over more than a century. However, gravimeters with a precision sufficient to observe hydrologic effects of the order of μGals, are a relatively recent development. Construction of several types of gravimeters with this order of sensitivity has been

undertaken roughly contemporaneously with the development of the SG, but the SG is the only instrument designed for continuous recording of gravity changes, and its precision is more than an order of magnitude better than any other instrument currently available (Crossley et. al. 1999).

Sources	Order of gravity changes
Solar and lunar tides, including Earth response	~300 uGal
Polar-tide effect	~10 uGal
atmospheric pressure effect	~20 uGal
ocean loading effect	0.3-5 uGal
terrestrial water storage variation	~10 uGal

Table 1.1: The magnitudes of temporal Earth gravity changes.

Terrestrial water storage variation is dominant in residual (non-tidal) gravity changes. Its gravity effects can be estimated by the Bouguer Slab approximation, which gives the attraction of an infinite plane of uniform density (Smith 2005):

$$\Delta g = 41.92 rh \qquad \mu Gal / m \tag{1.1}$$

where r is the slab density and h is the slab thickness. When applied to groundwater, it becomes:

$$\Delta g = 41.92 S_y \Delta H \qquad \mu Gal / m \tag{1.2}$$

where Sy is specific yield and ΔH is the water table changes in meters. The specific yield is defined as the volume of water that can be drains by gravity for a unit volume of aquifer material, and is expressed as dimensionless fraction or percentage. It's usually close to effective porosity, and can be estimated from pumping test data in many aquifer types. Equation (1.2) indicates that 1 μGal gravity changes is equivalent to water table changes of 24 centimeters with a porosity of 10%. This porosity and water table changes are common for many aquifers. Because the SG can detect gravity changes

smaller than 1 μGal, it is possible to observe groundwater changes from SG observations, and with coincident measures of water level changes in a nearby well, to estimate Sy.

The outline of the thesis is as follows. Chapter 2 presents a description of the development of a transportable SG system, including its mechanical configuration, moving and setup procedures, and SG site preparation. Chapter 3 presents the SG time series and summarizes data processing steps. Chapter 4 takes a look at the first SG operation for an experiment in the Edwards aquifer with preliminary results following.

Chapter 2: Development of a transportable SG system

The superconducting gravimeter (SG) has more than 40 years of history since its invention by John Goodkind and William Prothero at the University of California. Early production SGs were fixed to observing stations due to their bulky dewar and requirement of liquid helium. After a cryogenic refrigeration system was adopted in the late 1990's it became possible to develop an SG configured as a transportable field instrument, because 1) dewar size could be reduced greatly; and 2) helium loss was eliminated. This chapter includes an introduction to the SG gravity sensor and its electronics, SG temperature coefficient, configuration of a transportable SG system including its power and data arrangement, SG moving and setup procedures, and SG site preparation.

2.1 THE SG SENSOR AND ITS ELECTRONICS

The superconducting gravimeter, SGo047 (**S**uperconducting **G**ravimeter **o**bservatory model serial number **047**), is identical to other single-sphere GWR sensors delivered since the end of 2003. The gravity sensor unit (GSU), as shown in Figure 2.1, consists of a niobium spherical proof mass, 2.54 cm in diameter, levitated in magnetic fields produced by electric currents in a pair of superconducting coils. Capacitor plates positioned around the sphere sense the position of the sphere. When changes in gravity cause the sphere to move from its null position, a magnetic force produced by electric currents applied through feedback coils draws it back to its null position. Measuring the current through the feedback coil provide a measurement of gravity changes. Two tilt meters are mounted orthogonally inside the GSU. They provide signals to thermally controlled levelers, shown in Figure 2.2, to keep the instrument leveled so there is no

effect of tilt on measured gravity. GWR specifies precision for their current models as 10 nanogals (0.1 nm/s^2) or better, and drift rate below 1 microgal (10^{-8} m/s^2) per month.

The liquid helium tank (dewar, as shown in Figure 2.2) and refrigeration system keeps the sensor close to 4.2K to maintain the superconducting state, and allow the system to operate indefinitely on a single filling of liquid helium. When un-refrigerated, the dewar capacity lasts 20 days after each filling of 35-liters of liquid helium. Excess refrigeration capacity can be used to condense liquid helium from a standard high pressure gas bottle. Each 342 cu ft cylinder will produce ~10 liters of liquid helium. The liquefaction rate is about 1-2 liters/day.

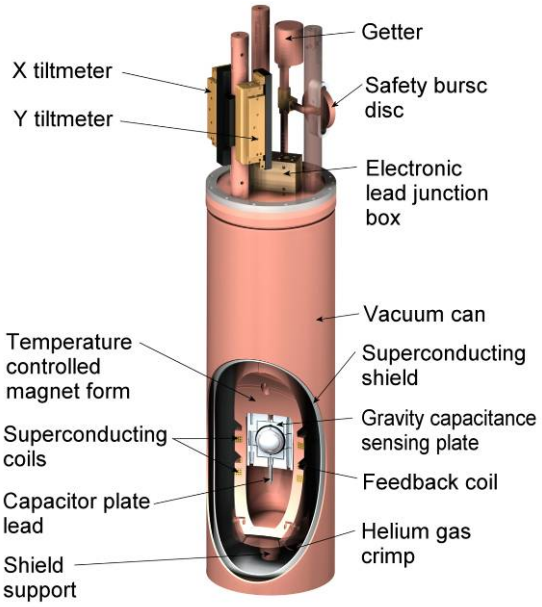

Figure 2.1: The gravity sensor unit of SGo047.

The refrigerator system consists of a helium compressor operated beside the dewar (typically several meters distant to prevent noise transmission to the gravity sensor), and a cold-head installed on top of the dewar (attached to the compressor via

flexible hoses). The cold-head has a life expectancy of more than 10,000 hours (1.1 year). During normal operation the cold-head often run much longer before requiring service. The compressor maintenance schedule requires exchange of the oil absorber module at 30,000 hour (3.4 year) intervals.

The liquid-helium dewar is connected to the cold-head on the top via a plastic diaphragm, which isolates vibration from the gravity sensor. At the bottom, it is supported by three posts: left X post, right Y post and rear post. The heights of post X and Y can be adjusted using precision micrometers and thermally controlled levelers, which are integral to the tilt compensation system. When the SG operates in a lab or in the field, all these posts should be in firm contact with the lab floor or solid ground.

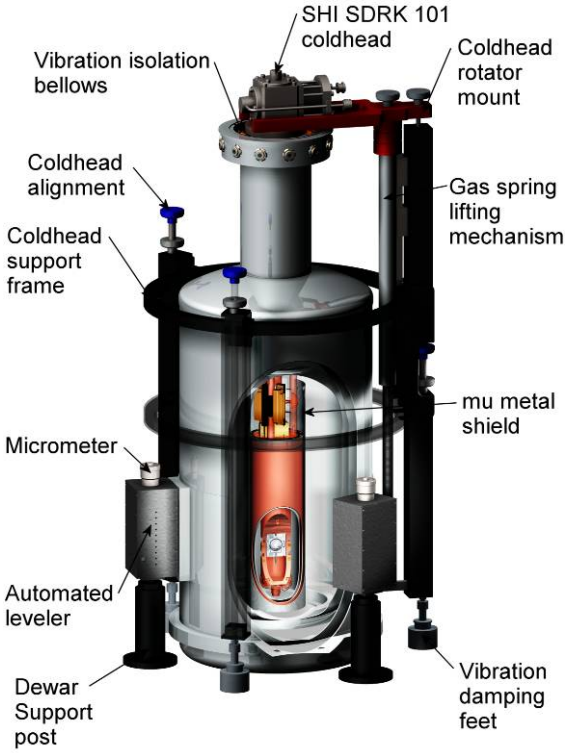

Figure 2.2: The liquid-helium dewar configuration of SGo047.

In addition to the automatic tilt compensation system, consisting of tilt meters mounted inside the GSU and thermally controlled levelers; a gravimeter electronics package (GEP-3); a current supply/heater pulser (DPS-3); a data acquisition controller (DAC); a digital voltage meter (DVM); and a computer to run user-interface and data logging software are shown in Figure 2.3. To prevent data loss and signal offsets in power failures, an Un-interruptible Power Supply (UPS) is provided for SG electronics and the computer.

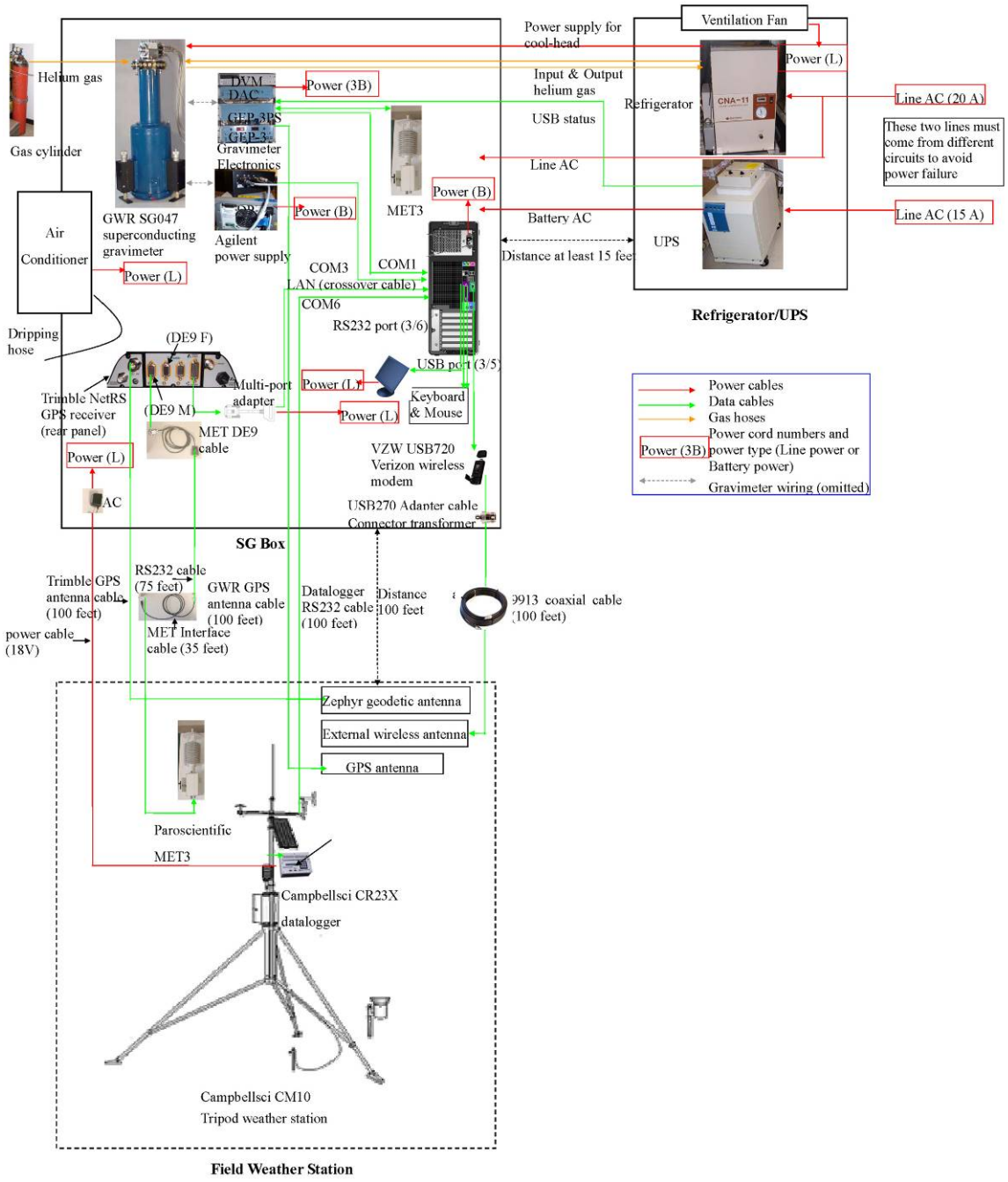

Figure 2.3: Configuration of transportable SG system. Solid-line rectangles represent two enclosures, SG box and refrigerator/UPS box. Red lines indicate power cables. Green lines indicate data cables. And yellow lines show hoses for helium-gas.

2.2 CONFIGURATION OF TRANSPORTABLE SG SYSTEM

The development work included integration of a full weather station, a geodetic GPS receiver with gravimeter SGo047 and implementation of data collecting and wireless data transfer.

The weather station, Campbell Scientific CM10 tripod weather tower, uses a variety of sensors, (Table 2.1), to get metrological information, such as temperature, barometric pressure, humidity, wind speed and direction, solar radiation, rain fall, and soil moisture content. It uses a data logger, Campbell Scientific CR23X (which can be programmed), to sample data up to 1Hz, store, and transfer data to a PC computer by a RS232 serial cable. In addition to the weather instruments, there are two GPS receivers and one wireless antenna, and a MET3 metrological measurement system (specially designed for GPS-meteorology) mounted on tripod tower.

The Trimble NetRS GPS receiver, integrated with paroscientific's MET3, can be used to calculate the amount of precipitable water vapor in atmosphere, and to provide vertical position control on the SG if that is needed in a specific application. A user-interface PC computer (UIPC) is used to collect data from all instruments (SG, GPS receiver and weather station), and for remote control and data transfer. Without liquid-helium loss, the transportable SG only needs minimum maintenance.

Sensor type	Model	Observations	Unit	Accuracy or sensitivity
Tripod weather station	CM10	7.2 feet with full leg extension		
Data logger	CR23X	24 single-ended analog inputs, 4 pulse counting channels, computer RS-232 port, programmable		
Barometric pressure sensor	CS115	Barometric pressure	mbar	0.3 mbar at 20ºC
Temperature and relative humidity probe	HMP45 C	Temperature Relative humidity	ºC Percentage	0.2ºC at 20 ºC 2% (0 - 90% RH)
Windset	Met One	Wind speed	m/s	0.12 m/s

	034B-L	Wind direction	degree	4°
Pyranometer	LI200X	Solar radiation	w/m2	0.2 kW/m2
Tipping Bucket Rain gauge	TE525	Rain fall	Mm	0.01 inch per tip
Water content reflectometer	CS616	Water content	Percentage	~2.5%

Table 2.1: Sensors for the field weather station. with their type, model, observations, unit and accuracy/sensitivity.

2.3. SG TEMPERATURE COEFFICIENT

Initial plans called for SG experiments in field settings in Central Texas and Arizona where ambient temperatures can reach 90º to 100ºF (32.2º to 37.8º C) in the day and drop a lot at night. It was therefore necessary to determine whether the SG gravity signal might be affected by such conditions. Considering the SG measures the voltage to obtain gravity change and the voltmeter may have a temperature coefficient, I conducted experiments to check the influence of temperature on SG measurement.

In our lab, the SG was operated under three temperature conditions: cold temperatures (around 63ºF/17.2ºC), high temperatures (around 90ºF/32.2ºC) and controlled temperature (at 80ºF/26.7ºC). They were regulated using different operation modes for the air conditioner inside the SG enclosure: always on, always off and thermal-controlled. Each condition lasted three days. The temperature inside the SG box was recorded by a Campbell Scientific 107L probe and the GEP3 chassis, as shown in Figure 2.4. In cool and high temperatures cases, the temperature inside the SG enclosure changed with ambient temperature. In the third case, the temperature undergoes only a small oscillation due to cycling of air conditioner.

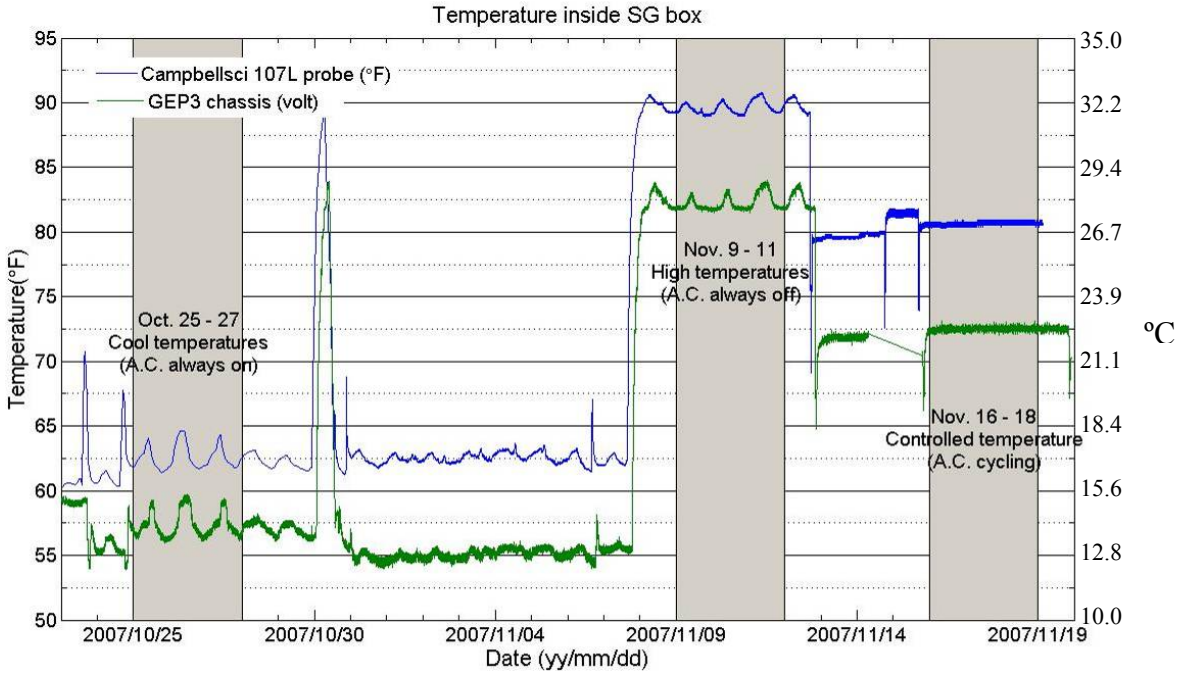

Figure 2.4: Temperature inside SG box during temperature-coefficient experiment. The experiment includes three temperature conditions: low temperatures, high temperatures and controlled temperatures. Each temperature condition lasted for three days.

The SG gravity measurement is shown in Figure 2.5. It is the gravity residual after removing Earth tides, atmospheric effect, residual tides and linear drifts (described in Chapter 3). For three temperature conditions, the gravity residual has the same noise level. Besides that, one minute samples of tilt balance are also shown in Figure 2.6. For cool and high temperatures, tilt X and Y varies between [-0.02 0.02] volt, like white noise. For controlled temperature (which is realized by cycling of the air conditioner inside the SG enclosure), there is strong oscillation in tilt balance with the same period as air-conditioner cycling. Such tilt oscillation may cause long-time resonance in gravity measurement, which should be avoided.

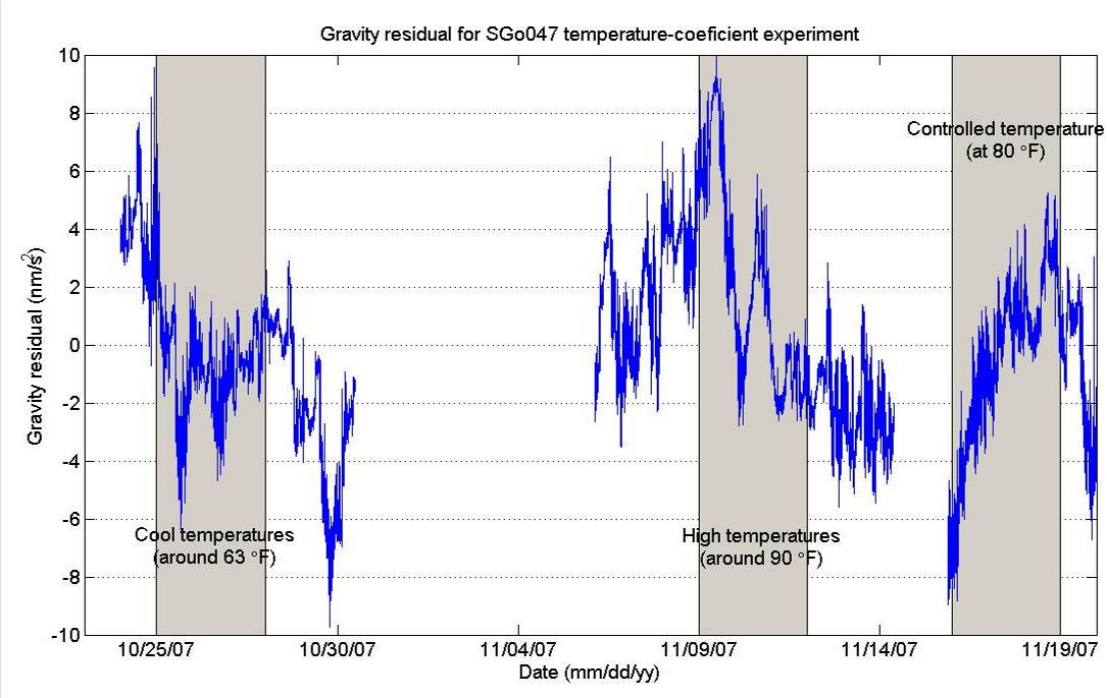

Figure 2.5: SG gravity residuals during temperature-coefficient experiment.

All these indicate that high or varying temperatures do not affect SG gravity measurement. However, it is better to operate the SG under a constant cool temperature while not using the air conditioner inside the SG enclosure because the cycling of temperature affects level control. Therefore, the air conditioning unit inside the SG enclosure was not used in the field experiments. Although the SG performance is not affected by high temperatures, the liquid helium compressor has stringent requirements for ambient operating temperatures. The preferred temperature is from 4º to 28ºC. Between 28º to 38ºC, the compressor will lose about 10% capacity, and there is danger of shortening the mechanic life of the unit as well. In Central Texas and Arizona, air temperatures easily exceed this range. In addition, the compressor produces a large amount of heat, it requires a cooling system of its own.

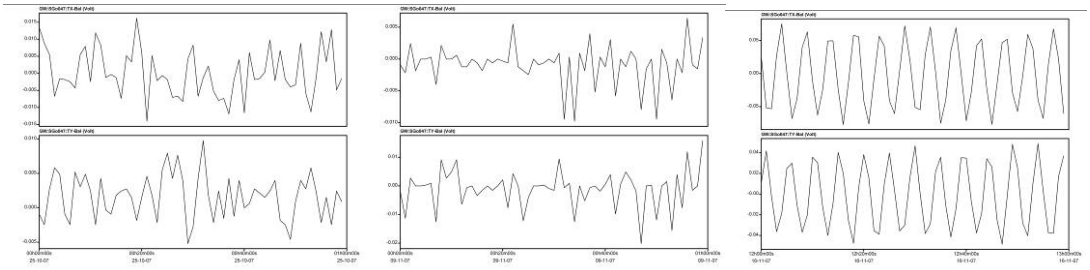

Figure 2.6: One minute samples of tilt X and Y balance during temperature-coefficient experiment. From left to right: cool, high and controlled temperature conditions.

2.4 POWER ARRANGEMENT

Besides the temperature requirement, the helium compressor has a stringent power requirement. Its maximum current is 15.1 amps at 100VAC/60Hz. This current requirement is such that wired power is necessary. Solar panel power is not practical in a field setting. In addition, it is necessary to have two dedicated circuits, one for the compressor, with capacity of 20 amps, and the other for the electronics, with the UPS serving as the power conditioner and backup supply in the event of power failure.

Figure 2.7 shows electrical wiring for our SG system. Electric power is supplied to refrigerator/UPS enclosure via two 20A/120V circuits, with power passed on to SG enclosure via a flexible conduit. In normal operations, total current requirements are below 20A, but exceed this following a power failure, as the UPS batteries recharge. Power failures can cause data loss and possible data offset if the duration exceeds the capacity of the UPS system. Therefore, one circuit supplies the UPS which powers SG electronics and is able to sustain data acquisition for several hours after a power failure. The second circuit provides surge-protected power to the cryogenic refrigerator compressor, cooling fans, and weather station. Loss of power on this circuit does not cause a loss of gravity data.

In addition to power failures, instruments must be protected from power spikes and surges by a surge protector, as in Figure 2.7. Because of large power consumption of the refrigeration system, it is not practical to backup the system for long periods with a UPS and batteries. Besides, the liquid helium acts as a ballast to maintain the SG at 4.2K during power failures. Therefore, maintaining uninterrupted power to the refrigeration system is not as critical as it is for the SG electronics.

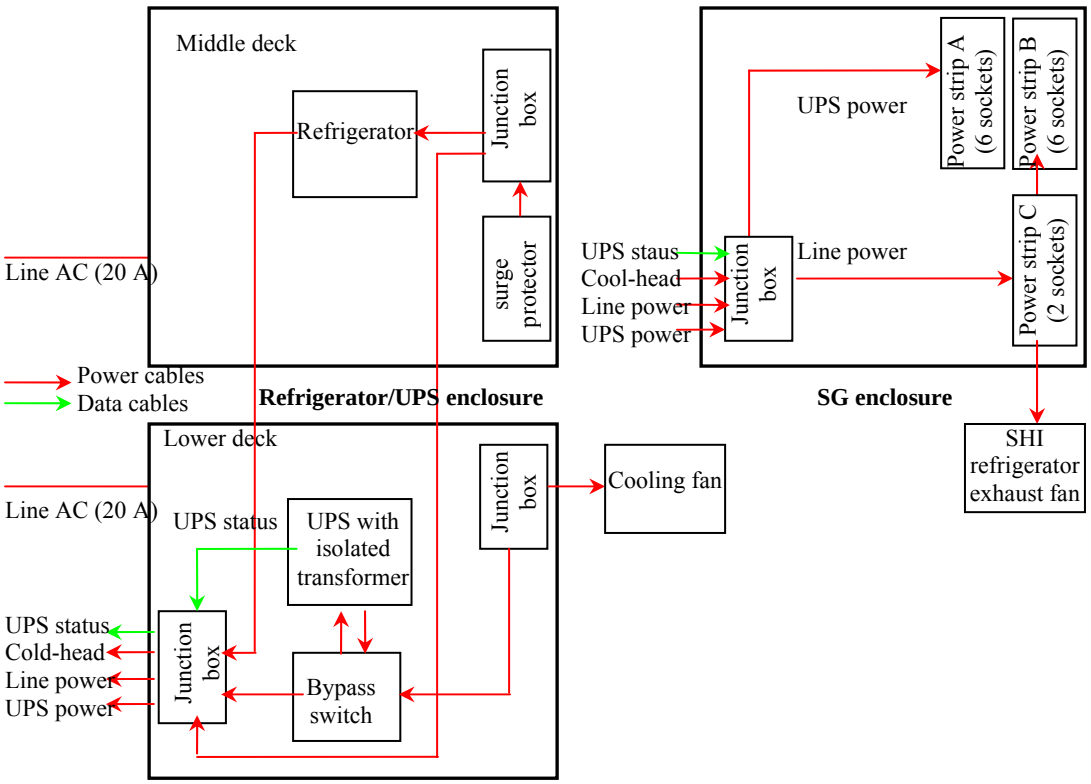

Figure 2.7: Electrical wiring of the SG box and refrigerator/UPS box.

2.5 DATA ARRANGEMENT

In our SG system, there are several instruments working together to provide a variety of information, including barometric pressure, integrated water vapor, meteorological data and gravity changes. Each instrument has its own data format, sampling rate and collection schedule. It's critical to have them uniformly arranged.

A command script, as shown in Appendix C, runs at midnight (Universal time) to collect the full day of measurements from all instruments, and saves them into files with names indicating date and instrument. Then, it uploads a copy of all files to a remote server using a wireless internet connection. In later processing, I convert all time into UTC (Coordinated Universal Time), resample data with interval of 1 minute, and save all data into one file in TSOFT format.

2.6 MODIFICATION FOR TRANSPORT

Our SG system has been configured for field use. Taking advantage of the relatively small size of the dewar, all system components can be packaged into two enclosures (E1 and E2), constructed from angle and sheet aluminum, secured by screws and welds and supported by adjustable legs at each corner. Enclosures provide physical protection, facilitate control of temperature and humidity, and allow relatively simple handling during transport. E1 and E2, with instrument installed, are shown in Figure 2.8 and 2.9. Their structures are also shown in Figure 2.10 and 2.11.

Enclosure E1 contains SG dewar, cold-head with support frame, SG electronics, GPS receiver, barometer and PC computer. SG electronics, GPS receiver and barometer are mounted on racks. The cold head frame is secured to the base of E1 with isolation mounts provided by GWR. The dewar is supported on three aluminum posts (provided by GWR) secured to a large aluminum plate. The three posts pass through the base of E1 and rest on the concrete floor. Enclosure E2 contains the cryogenic refrigerator

compressor, Un-interruptable Power Supply (UPS), and lightning surge protector. Temperature inside E1 was originally designed to be regulated by a thermo-controlled 0.4 kW (1500 BTU) heating/cooling unit mounted at the rear, but interference with thermal leveling, noted earlier, meant that it was not used in field operations. E2 is cooled by ambient air via a top-mounted exhaust fan. E1 and E2 are joined by two 15 m refrigeration hoses, and a flexible conduit carrying UPS data cable, cold-head power cable, and power cables. A 100-foot flexible conduit carrying antenna, data and power cables joins E1 with the weather station. E1 has a dimension of 36"x30"x69" (WxDxH), and weights about 250 lbs with SG and instruments installed. E2 has dimension of 38.5"x32"x56" (WxDxH), and weights about 450 lbs when refrigerator and UPS are loaded. Due to enclosures' size and weight, hand operated jacks or forklifts are required to move them.

E1 and E2 can be transported with instruments installed. To keep the dewar upright and avoid liquid-helium spill over, the dewar must be clamped to its supporting frame. Cold-head frame legs are connected by L brackets on the frame legs with the dewar brackets, providing a rigid connection and the majority of support to the dewar weight. Figure 2.12 shows the process of attaching the brackets to the legs. Initially the procedure was to lower the cold-head and secure it to the dewar neck using 4 machine screws, but this was found to be unnecessary, and later moves were accomplished by removing the cold-head, then securing the dewar only at the base. Then the L brackets on the legs are lowered to meet the dewar brackets, and the L brackets tightened on the frame legs. The last step is to secure the L brackets to the dewar brackets. The rear bracket is secured using stainless steel hose clamps strapped around the leg containing the lifting spring.

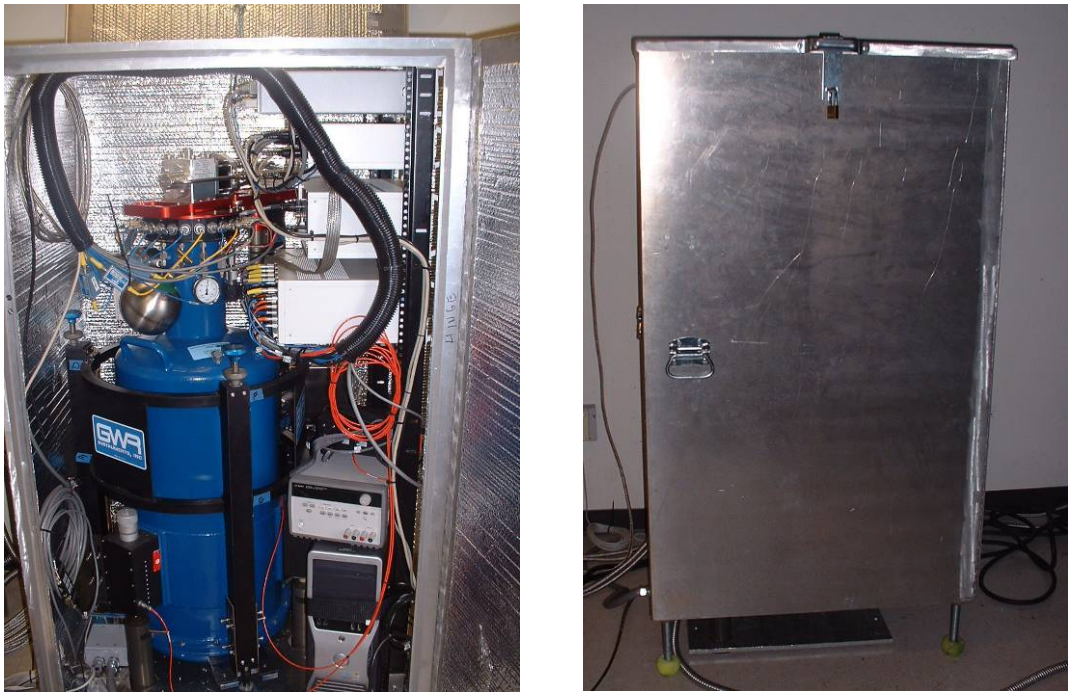

Figure 2.8: Internal and external view of enclosure E1.

Figure 2.9: Internal and external view of enclosure E2.

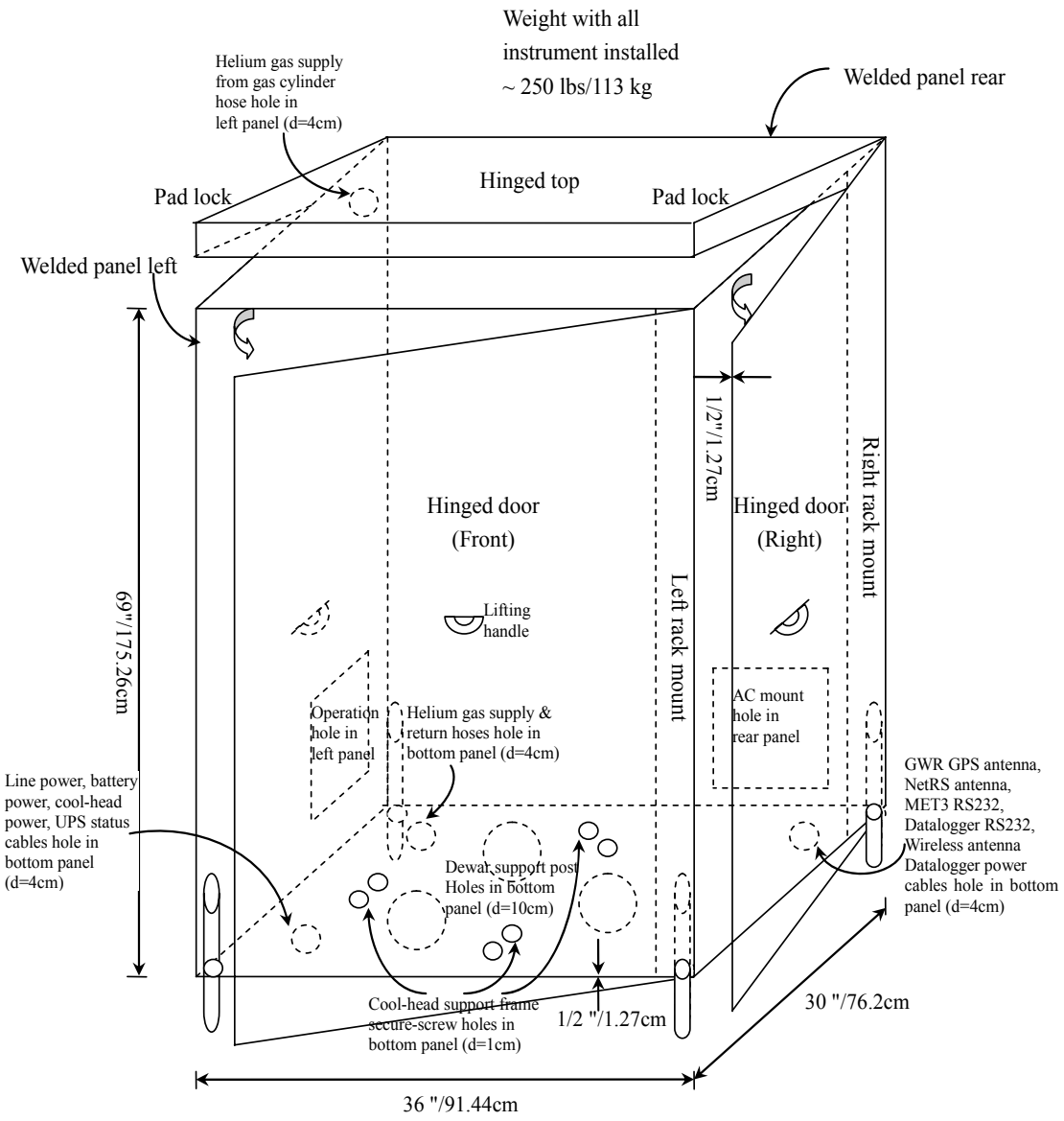

Figure 2.10 Enclosure E1 structure.

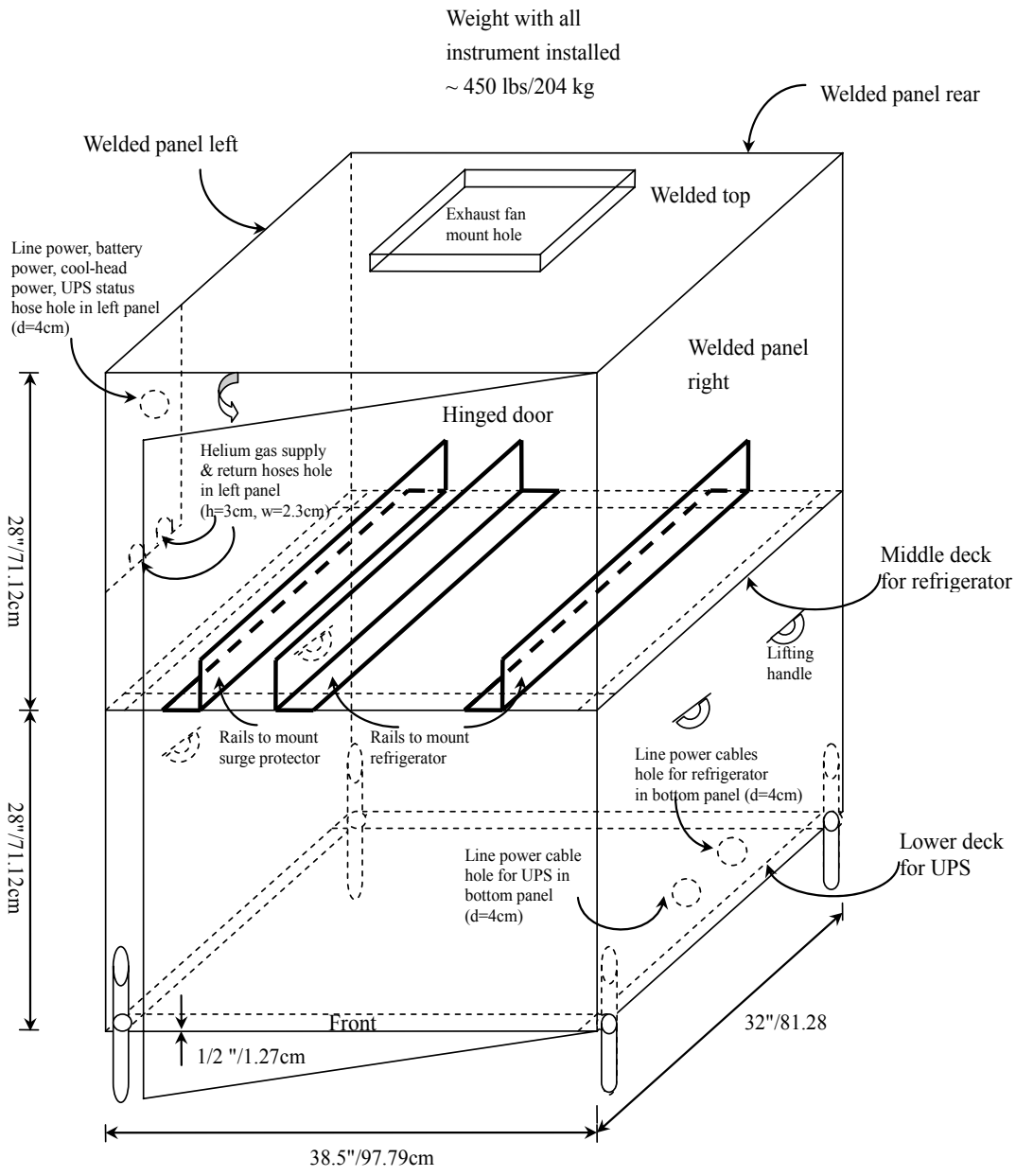

Figure 2.11: Enclosure E2 structure.

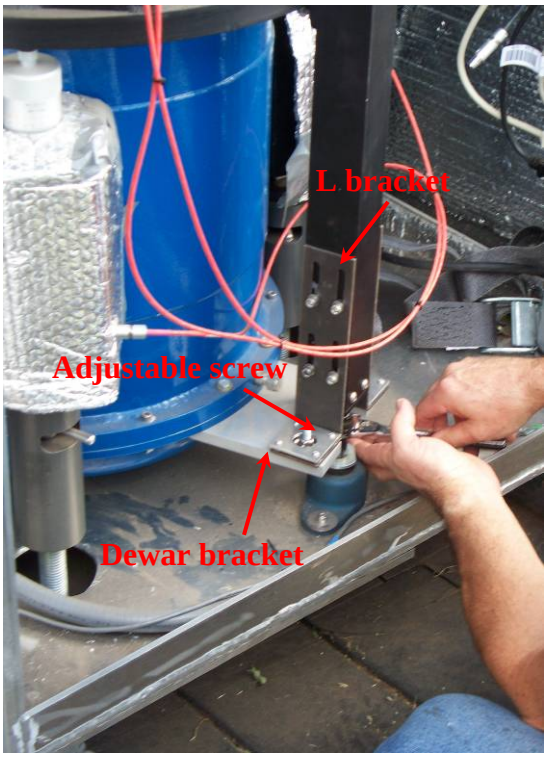

Figure 2.12: SG dewar clamping to cold-head support frame.

2.7 SG MOVING PROCEDURE

Enclosures E1 and E2 can be transported by a truck with instruments installed and cables connected. Only hoses and cables joining the two enclosures need to be disconnected. The weather station can be transported with sensors mounted and tripod retracted. That means the entire system can be transported with one load on a medium truck with either a hydraulic lift gate or a loading ramp.

Before moving, about 6 hours are required for the following operations:

1. Shut down entire system (turn off the refrigerator, close UI software and shut down the computer).
2. Disconnect power cords, gas hoses with data cables joining E1 and E2

3. Remove the cold-head and cover the dewar with a phenolic lid, following GWR manual procedures.
4. Clamp the dewar to the cold head frame
5. Raise E1 about one-half meter with portable lifts to remove the three aluminum posts and baseplate assembly from below
6. Raise E1 and E2 onto dollies and load them onto a truck.
7. Transport E1 and E2 to a new location

At the new location, do the reverse to unload and reassemble the SG system.

Our experience proved that SGo047 can be transported with proof mass levitated, and ~4K temperatures maintained by the liquid helium bath. For safety, it's recommended to seal all openings on the dewar neck. When open to the atmosphere, very cold conditions can cause air to be sucked into the dewar, freezing all gases and water, and risking an explosion. The dewar is isolated via the plastic diaphragm so that a short move, where conditions are being monitored closely, can be accomplished with the diaphragm in place. For longer moves where transport conditions might cause a puncture, it is necessary to remove the diaphragm and place the phenolic plastic lid over the dewar opening. Liquid helium levels should be somewhat less than full, below about 95% prior to moving to prevent liquid He spill over during moving.

2.8 SG SETUP AT A NEW LOCATION

After the is SG reassembled at the new location, an additional 8 hours are required to set up the system in operation mode. It includes dewar re-leveling, sphere re-centering and tilt minimization.

2.8.1 Dewar re-leveling

Inside the gravity sensor unit, two tiltmeters are placed orthogonal to each other. However, the dewar is supported by an equilateral frame. Therefore, a change in the X micrometer will produce a tilt signal on both the X and Y tiltmeter. When tilt controls are switched to RUN mode, the dewar keeps the system at the level which has minimum effect on gravity, the 'tilt null', with thermal auto-leveling system.

Re-leveling can be done in the following way:

1. Set gravity sensor in Strong Feedback mode (BD=3), then set both X & Y micrometers to 500.
2. Switch X & Y tilt control to "Temperature Feedback", set the X & Y tilt meter BD= 3, and set the X & Y RESET to preset values.
3. Set the panel to display tilt X & Y balance.
4. Perform sensitivity check to ensure cables are connected properly.
5. While observing the tilt X and tilt Y balance readings, adjust the rear screw until their absolute values are equal, i.e. $|Vy| \approx |Vx|$. .
6. If the absolute value is > 3 leave BD=3 and proceed to next step. If the absolute value is < 3, set BD=4, and adjust the rear screw to achieve $|Vy| \approx |Vx|$.
7. Null both the Tilt X and Tilt Y Balance signals using the X and Y micrometers. *This is an iterative process due to the triangle support structure. That means you need to use X and Y micrometer in turn, and get them closer to zero while keeping* $|Vy| \approx |Vx|$. *If you find one micrometer is very loose when you turn it, that means the post doesn't take dewar weight. The dewar contacts somewhere with the frame. Make sure it's also clear between dewar neck and cold-head.*
8. Continue to null Tilt X and Y balance while increasing BD=5.

9. Use the micrometers to carefully null the Tilt X Bal and Tilt Y Bal within 0.5 V on Tilt BD=6.
10. Record the X & Y micrometer values.
11. Switch X & Y tilt control to "RUN", and set the X & Y tilt meter Bridge Drive BD=7.

2.8.2 Sphere re-centering

Due to the gravity difference between old and new locations, the spherical proof mass may change its null position and put the gravity feedback signal beyond the range of the system. Therefore, the second step is to re-center the sphere with currents in magnetic coils. This procedure has been changed following the rebuilding of gravity sensor and addition of a centering coil. A formal written procedure for this will be prepared by GWR.

2.8.3 Tilt minimization.

The gravimeter is configured to measure the component of local gravity along the direction of the local vertical. Tilt minimization is to find this position and keep the system along it. It should be done first using micrometers, then using thermal levelers.

2.8.3.1 Tilting using micrometers.

This procedure needs can be done in Medium Feedback (BD=6) or RUN (BD=7) mode.

1. Switch Tilt X and Y Control to Temperature Feedback and wait for Tilt X and Y Powers to be stabilized around 7V.
2. Record current micrometer reading and gravity signal.

3. Forward/Backward tilt +/- 4 mills. Each time, move X and Y micrometers in the same direction by 4 mills to produce a forward/back tilt. Record the micrometer reading and gravity signals on a strip chart.

   Tilting exercises a mode of oscillation of the sphere with a period of about 2 minutes. Therefore, you need to record 2 to 3 cycles to estimate the trend line of the midpoint of the oscillation. When you are tilting in the correct direction toward the tilt minimum, the gravity signal will move in the positive direction. Otherwise, you're tilting in the wrong direction.

4. Continue to tilt the dewar until the sign of the steps reverse direction as the gravity signal goes over a maximum.
5. Make a graph with the positions of the X and Y micrometers along the horizontal axis and change in gravity signal along the vertical axis. Draw a straight line to determine the tilt null and record the values for X and Y micrometers.
6. Set X and Y micrometers at these values and record the gravity signal for several minutes to establish a baseline.
7. Do the same for side to side tilt +/- 2 mills. Moving the X and Y micrometer in opposite directions produces a left/right or side to side tilt.
8. Record the new X & Y micrometer values.
9. Set the X & Y micrometers to the new values and null the Tilt X & Y Balance using the X & Y Tilt Resets.
10. Switch both the Tilt X and Tilt Y Controls from Temp FB to RUN.

2.8.3.2 Tilting using thermal levelers

This procedure must be done in RUN (BD=7) mode. Make a chart using a constant step of 40 hex and calculate the X-Reset values with three increments above and below the starting X-Reset value determined in Fine Tilt using micrometers.

1. Record the gravity signal.
2. Decrease the X-Reset by -0C0 so that you will start at the top of your table.
3. Let the gravity signal and X Heater power stabilize. It takes about 20 minutes. Record the gravity signal.
4. Increase the X-Reset by -040 and let both the gravity signal and X Heater power stabilize.
5. Continue the step above until you end at the bottom of the table.
6. Make a graph with the X-Reset along the horizontal axis and change in gravity signal along the vertical axis. Draw a straight line to determine the X-reset value that has maximum gravity signal.
7. Set the Tilt X-reset value to the value determined above.
8. Let the system stabilize.
9. Repeat this process using the Y-reset function, while recording the gravity signal and the Tilt Y Heater power.
10. Set the Tilt Y-Reset value to the value determined.
11. Carefully record the final values of the X-Reset and Y-Reset.

After all these steps, the SGo047 now can be switched to RUN mode, and begin data recording.

2.9 SG SITE PREPARATION – THE GREEN EMERALD TERRACE EXPERIMENT

A field experiment was conducted in South Austin at a site on City of Austin lands near the end of Green Emerald Terrace. The location is adjacent to the well 58-

49-940 shown in the map of Figure 2.13. The site contained an electric power pole, but permanent structures were not permitted, requiring construction of a monument that could be removed after the experiment. The monument consisted of drilled 1 inch steel rods cemented into outcropping limestone, and instrument sheds (plastic garden sheds) were placed around it with plywood floors.

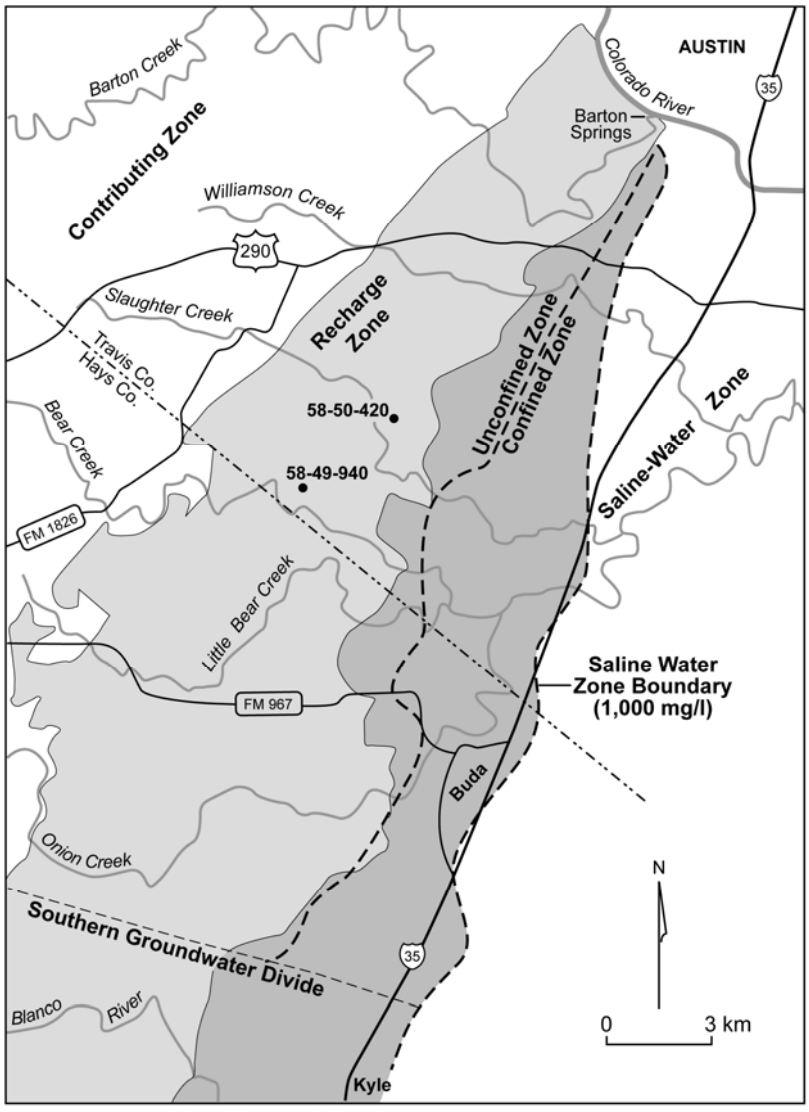

(Hunt, 2004)

Figure 2.13 The SG location during Green Emerald Terrace Experiment, adjacent to well 58-49-940, in a hydrological map of Edwards Aquifer, Central Texas.

Figures 2.14 and 2.15 show the schematic layout of the two sheds (S1 and S2), which host enclosures E1 and E2 at the Green Emerald Terrace site. S1 and S2 are placed back to back. Each is a Rubbermaid 3.5'x7' storage building mounted on 4'x8' plywood deck. S1 and S2 are cooled with an air conditioner in S2. A gable-mounted fan, controlled by thermostat switch in E1, takes exhaust heat out from S1 and passes cool air to it through two holes on side panels at bottom. Those two holes are also used to pass through refrigeration hoses and cables from the weather station. Three 20-amp circuits provide electrical power, two for the refrigerator and gravimeter, and another one for the A/C.

The SG gravity sensor is very sensitive to tilt and elevation changes transferred from ground surface. Therefore, SGo047 must stand on a monument cemented to hard rock, as shown in Figure 2.16. SG dewar is supported by three aluminum posts provided by GWR. Each post is mounted on one-inch rod, which is cemented into hard rock about 18 inches/45.72 cm. And each pillar goes though the shed floor and plywood deck through a 3 inch clearance hole. Two 3/4 inch (1.9 cm) aluminum plates are used to align these pillars. The lower one is used during cementing and the upper one is used during gravimeter installation. The heights of two plates are adjustable during gravimeter installation. Besides, the enclosure stands on the shed floor with four adjustable legs at each corner.

Figure 2.17 shows all gravimeter installation completed. The picture is taken in November 2008 at the Green Emerald Terrace site, where our SG collect its first long time series throughout June 2009. As shown in Chapter 4, there are several offsets in gravity data. Some of them are caused by the dewar neck touching the cold-head supporting frame as a result of wood floor bending under enclosure weight. Another coincides with a rain event in area around Mar. 15, 2009. The gravity jumps from 0V to

-4V with tilt balance move away from null position (0 V), and beyond the range (10 V). Such phenomena can be explained by rainwater expanding the fractures and clay inside the limestone base and tilt pillars that supporting the dewar. Such problems can be reduced in future SG deployment by pouring a concrete platform around the monument to protect pillars and securing cold-head frame to it. This was an important lesson.

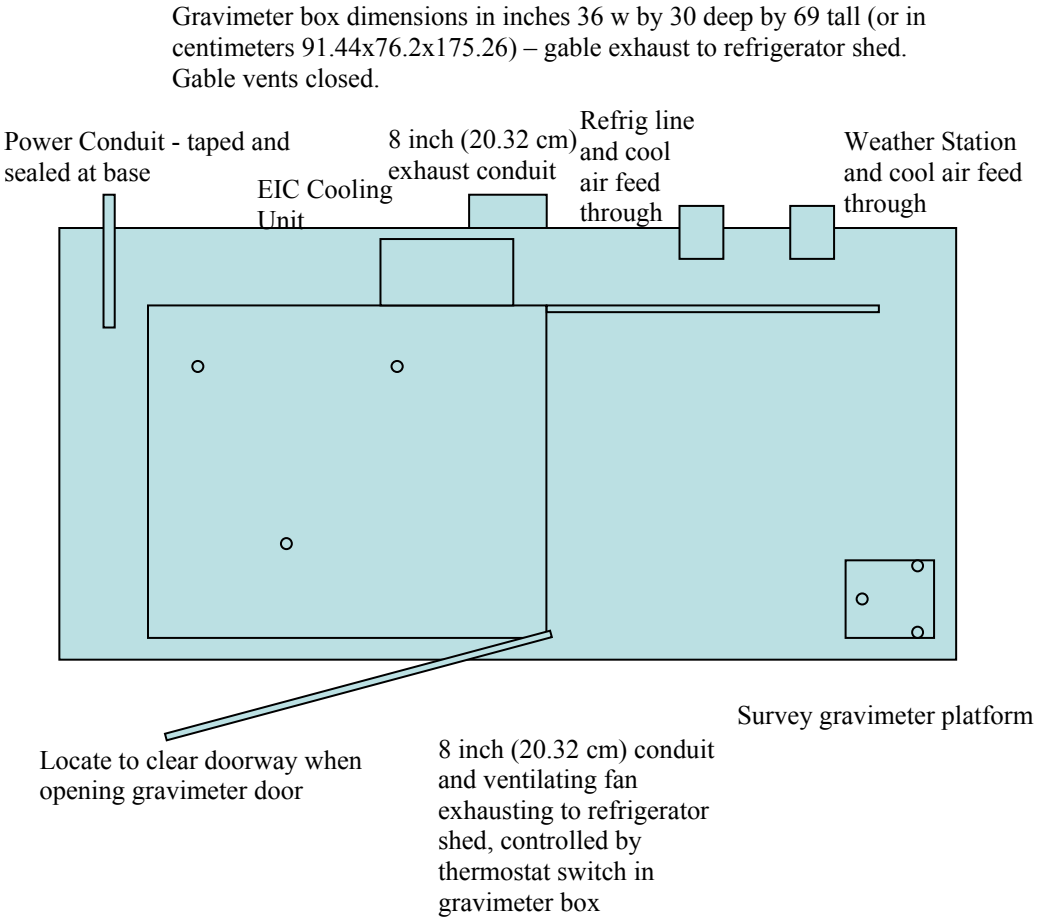

Figure 2.14: Gravimeter shed (S1) layout at site of Green Emerald Terrace. Gravimeter box and shed are drawn in same scale. The shed is a Rubbermaid 3.5'x7' (1m x 2.1m) mounted on 4'x8' (1.2m x 2.4m) plywood deck. There are two holes on side panel for refrigerating hoses and weather station cables to go through, and one exhaust conduit on gable to refrigerator shed. The power conduit at left bottom is used to pass power from refrigerator shed.

Refrigerator UPS box dimensions in inches 38.5 w by 32 deep by 56 tall (or in centimeters, 97.79x81.28x142.24), with additional 12 (30.48cm) for top ventilator. Receives exhaust from the gable mounted fan. Leave one gable vent open

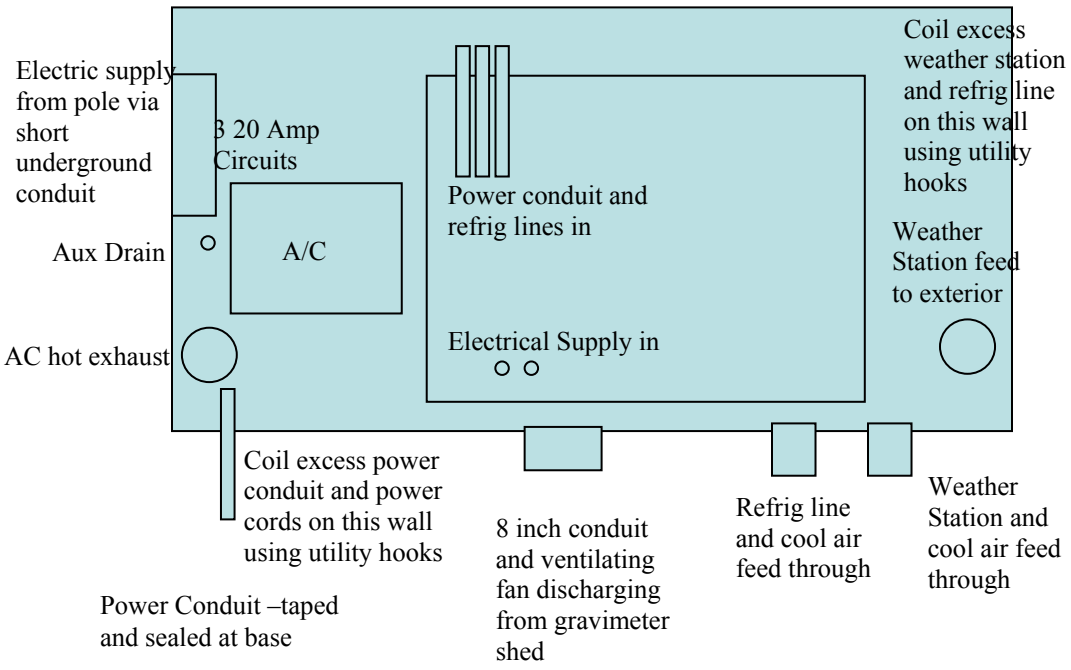

Figure 2.15: Refrigerator shed (S2) layout at site of Green Emerald Terrace. Refrigerator box and shed are drawn in same scale. The shed is a Rubbermaid 3.5'x7' (1m x 2.1m) mounted on 4'x8' (1.2m x 2.4m) plywood deck. There are two holes on side panel for refrigerating hoses and weather station cables to go through, and one exhaust conduit on gable to gravimeter shed. The power conduit at left bottom is used to pass power from to gravimeter shed. On the floor, there are two holes for AC exhaust and weather station cables. The air conditioner is used to cool-off the shed and let the refrigerator operated under normal temperature. Three 20-amp circuits provide electrical power to the refrigerator, gravimeter and air conditioner respectively.

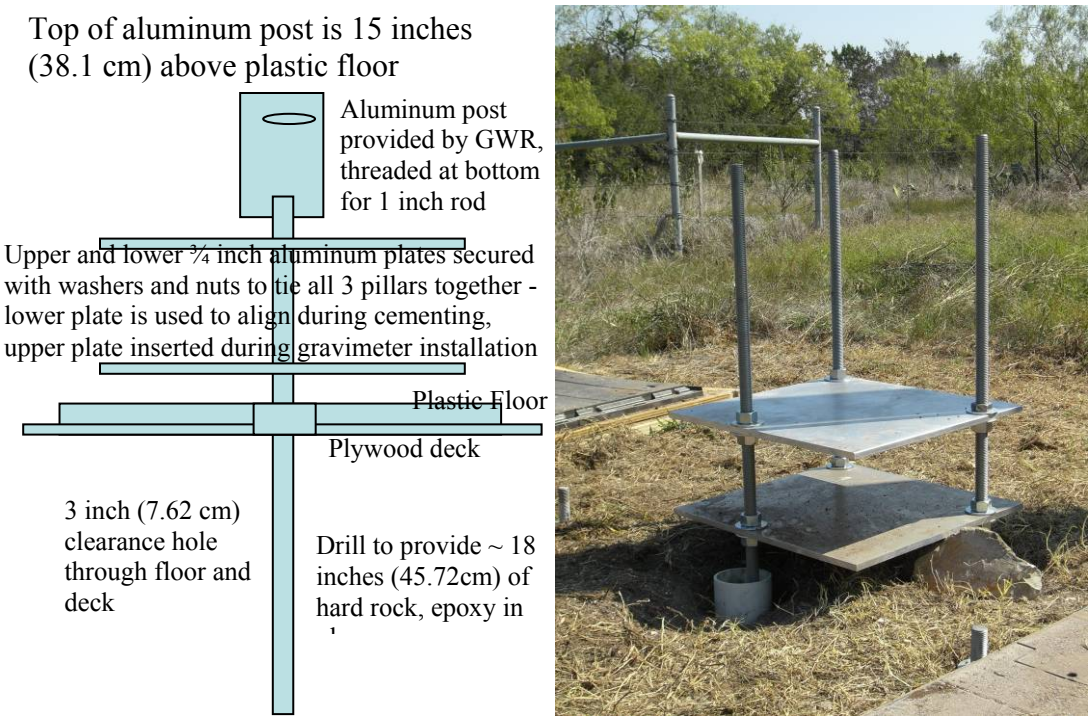

Figure 2.16: Gravimeter monument at site of Green Emerald Terrace. Left panel is the sketch diagram (not to scale). There are three post supporting SG dewar and mounting on one-inch rod, which is cemented into hard rock about 18 inches (45.72 cm). Two ¾ inch (1.9 cm) aluminum plates are used to align three pillars. The lower one is used during cementing and the upper one is used during gravimeter installation. Right panel is the picture taken before the floor laid and gravimeter installation. The heights of two plates are adjustable during gravimeter installation.

Figure 2.17: Pictures taken at Green Emerald Terrace when gravimeter installation completed. The left panel shows gravimeter shed, shed door and enclosure door opened. Right panel shows refrigerator shed.

Chapter 3: SG data processing

The purpose of this chapter is to give an overview of SG data processing and to present a standard procedure for processing when the main goal is to investigate gravity changes due to hydrologic variation.

SG data analysis methods are fully described in the published literature (Van Dam and Francis 1998, Neumeyer et. al. 2006), and a full range of software and other processing tools is publicly available. Here, those tools are described and used to examine the SG data taken during the development and testing period, from October 2007 to October 2008. A subsequent chapter describes operations and results from the Edwards Aquifer (EA) field site, beginning November 1, 2008. The test and development period included operation within the Geology Building (GB) basement on the University of Texas Austin campus through March 2008, and then at the UT Pickle Research Campus (PRC) prior to the move to the EA site. There are various breaks in each series but the PRC series is the least contaminated by such interruptions.

3.1 TIME SERIES OVERVIEW

A SG provides a high precision measure of gravity change at a fixed point as a function of time. Units of gravity are acceleration and usually given in SI units of meters per second squared. Gravity at Earth's surface has a mean value of about 9.8 m/s^2 and SG precision is better than 1 part in ten billion, or about 1 nm/s^2. Thus 1 nm/s^2 is the convenient SI unit used in the discussion below. One μGal, a traditional gravity unit equals 10 nm/s^2. Records with this precision are expected to contain a number of signals with amplitudes of tens to thousands of nm/s^2 including: Earth Tides, both solid body tides and ocean load tides, seismic waves, gravity disturbances from nearby sources (vehicles, construction, maintenance visits to the SG), atmospheric effects (including

direct attraction and loading effect), instrumental drift, and polar motion. After removing all of these, gravity changes from groundwater and other sources should remain. The SG, and all relative gravimeters, such as mechanical spring instruments like the LaCoste-Romberg (LR), requires calibration. The fundamental measurement provided by the SG is a voltage proportional to gravity change. Although the SG manufacturer provides a nominal calibration factor, estimation of this factor is an important element of the time series analysis discussion

Figure 3.1 shows the SGo047 time series for the entire development and test period. The first part of the series is taken immediately after transport from the GWR factory in San Diego by truck (with the SG maintained in a superconducting state) on September 30 2007. The series ends in September 2008, prior to transport to the Edwards Aquifer site. There are five visible gaps in the time series. The first four are due to power failures from overloaded building circuits. This problem was fixed by rewiring to distribute the load over two circuits. The first gap is followed by an offset due to sphere sticking after the power was off several days. The last gap occurs during SG transport from the Geology Building to the Pickle Research Campus, followed by an offset as the sphere was re-centered after the move. Other gaps were due to brief power failures and didn't create offsets in data record. The GWR data logging system provides two time series. One is original voltage data sampled once per second, and the other is samples every minute, as in Figure 3.1. One minute samples are obtained from the 1 second samples by low pass filtering. For any hydrologic or similar application, 1 minute samples are sufficient and will be used in all subsequent discussions.

3.2 DATA PROCESSING

TSOFT is a Windows based software package developed at the Royal Observatory of Belgium, for the analysis of time series and Earth tides (Van Camp and Vauterin 2005). Most of the discussion here uses TSOFT functions, though some steps are also performed with MATLAB.

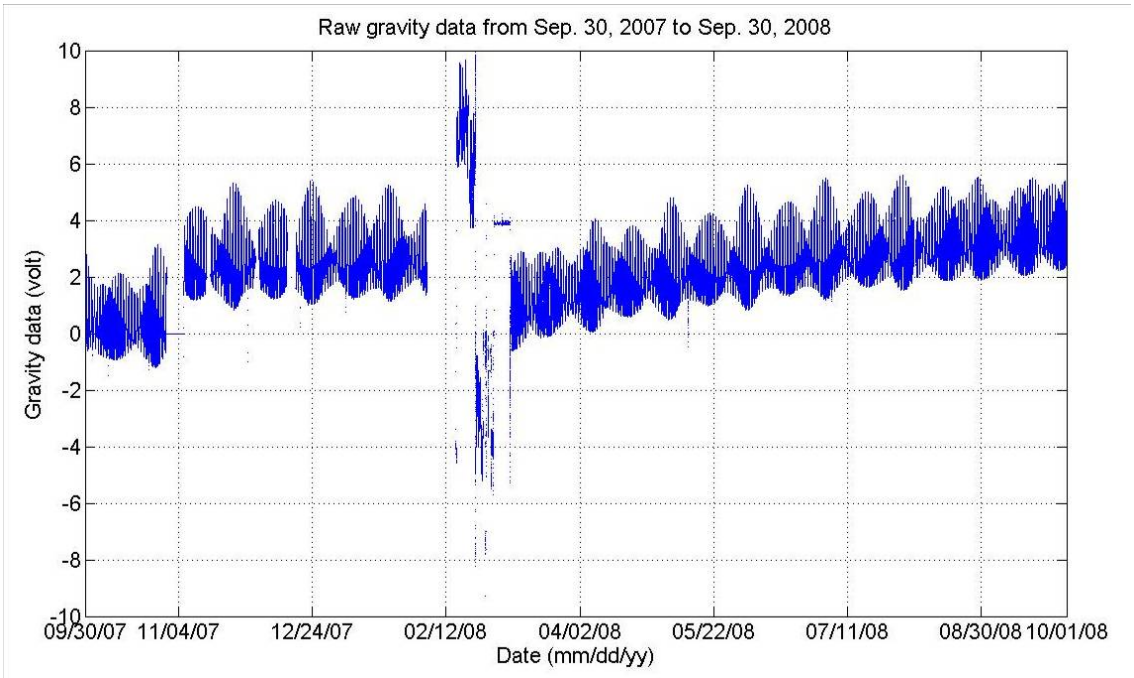

Figure 3.1: One-year SG time series taken at the GB and PRC sites, from Sep. 30 2007 to Sep 30 2008.

3.2.1 Data preconditioning

The first step is to remove gaps, steps and spikes in the time series, called preconditioning. In most cases, gaps and steps can be corrected automatically using TSOFT functions. Spikes can be automatically detected using various filters to locate points where deviations are greater than a preset value. Figure 3.2 shows the result of

preconditioning for data in Figure 3.1. Further correction of offsets and spikes can be done later if problems are evident, for example, after tides are removed.

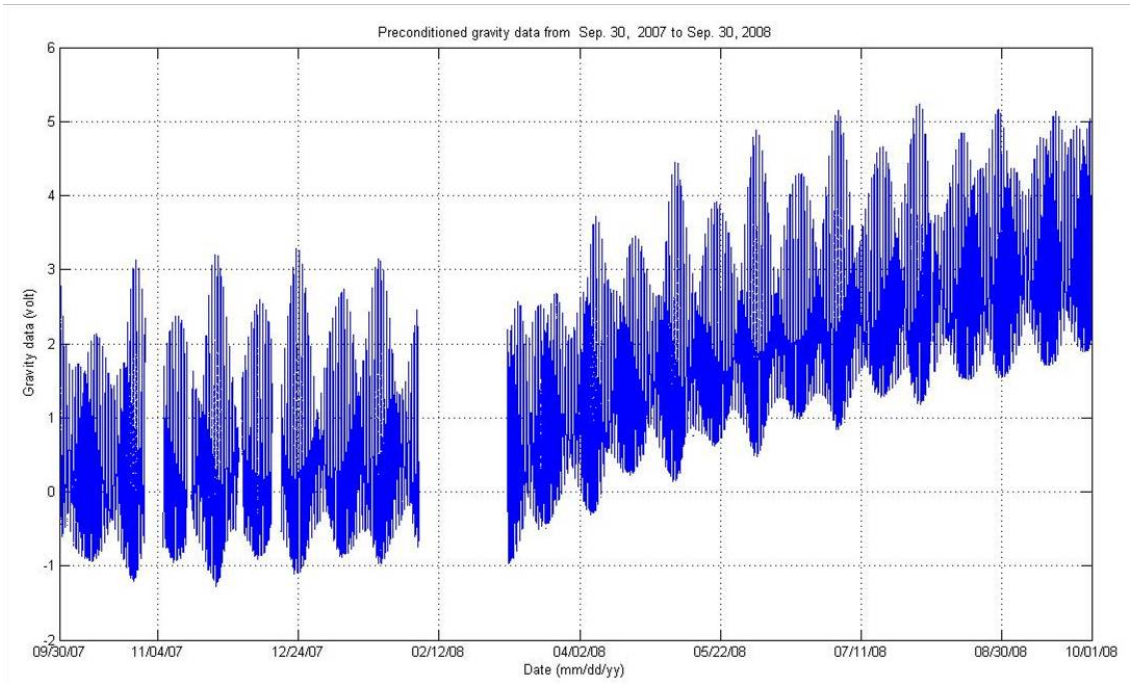

Figure 3.2: Preconditioned SG time series taken at the GB and PRC sites. Spikes are automatically corrected by TSOFT. Steps are manually corrected.

3.2.2 Earth Tides and Calibration

The next step is to remove Earth Tides, the largest signal in the SG record. Earth Tides are largely predictable from theory, so can be used to calibrate the SG. Alternatively, side-by-side operation with an absolute gravimeter or another calibrated SG provides a calibration method. The calibration factor provided by the factory for SGo047 was -748.54 nm/sec^2/Volt. The value obtained in the analysis below is -734.1 nm/s^2/volt, differing from the factory value by about 2%. In hydrologic applications, for example in estimating specific yield, even a 2% calibration factor uncertainty is relatively small compared to other sources, and the uncertainty is reduced below 1% in the analysis

of longer time series than done at the factory. In the discussion below, the sign of the calibration factor is understood to be negative in all cases, though some of the graphs show only its absolute value.

TSoft provides several functions to estimate a calibration factor, including a moving-window regression to find the best least squares fit between theoretical and observed tides, and examination of the calibration factor as a function of frequency. They are used in GB and PRC time series with the WDD Earth tide model (which is described below). The general results are that calibration does not appear to change significantly at the two sites, as shown in figure 3.3ab and 3.4ab. Thus calibration remains relatively unchanged despite transport and sphere re-centering associated with the move from GB to PRC.

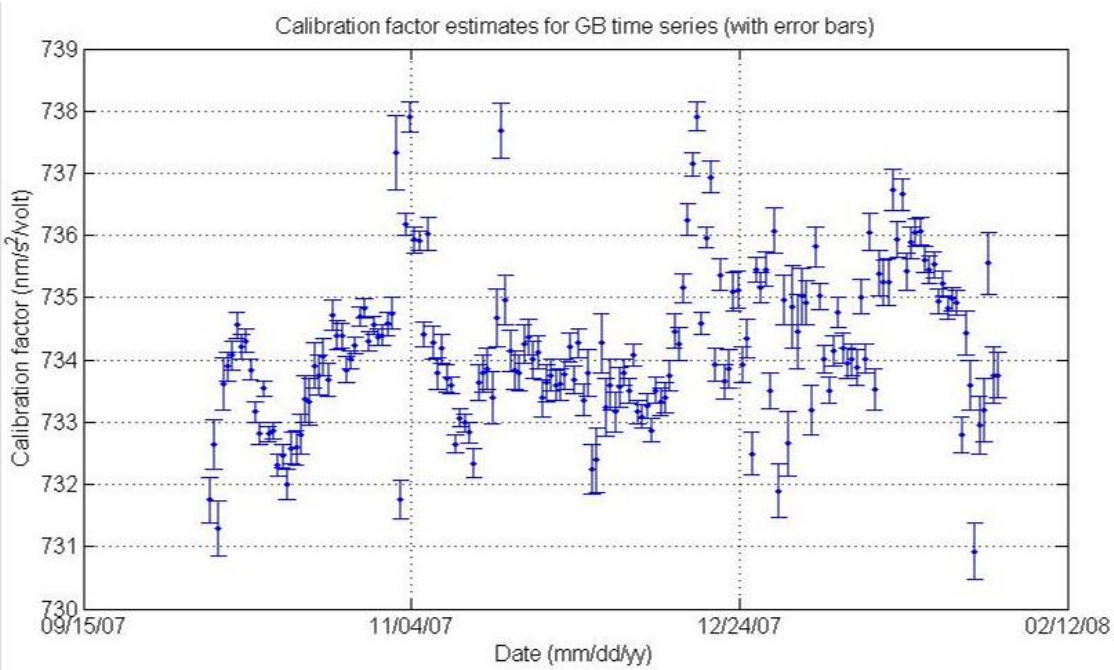

Figure 3.3a: Time variation of the estimated calibration factor (with error bars) for the GB time series. The estimate is based on the best fit to the predicted Earth tides (WDD) from a moving overlapping window regression of 10000 minutes (about 1 week) and windows separated by 1000 minutes. The mean calibration for the entire period, excluding the first week (when drift was rapid) is -734.15 nm/s2/volt (STD = 1.12) – a simple mean of all values and -734.11 nm/s2/volt (STD = 1.20) – a weighted mean using reciprocal variances as weights.

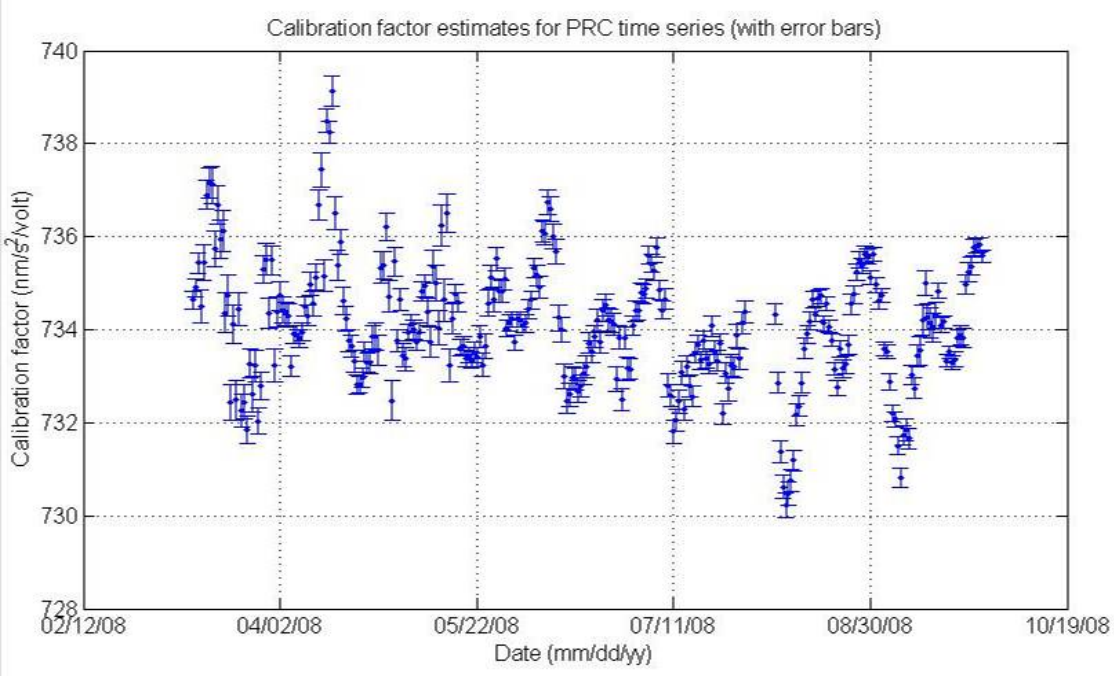

Figure 3.3b: Time-dependent variation of calibration factor (with error bars) for the PRC time series. The estimate is based on the best fit to the predicted Earth tides (WDD) from a moving overlapping window regression of 10000 minutes (about 1 week) and windows separated by 1000 minutes. The mean calibration for the entire period, excluding the period in late July associated with a power failure is 734.07 nm/s2/volt (STD = 1.31) – a simple mean of all values, and 733.87 nm/s2/volt (STD = 1.37) – a weighted mean using reciprocal variance as weights.

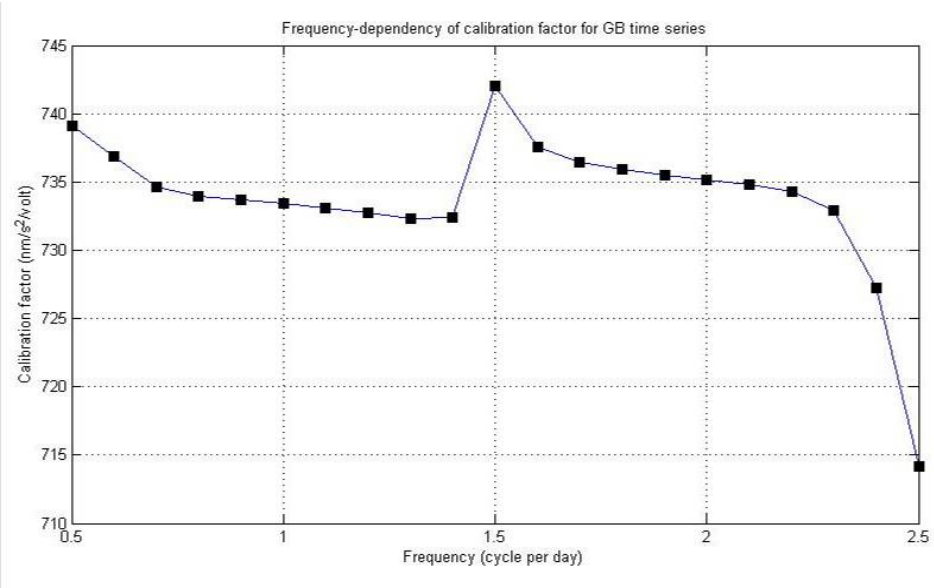

Figure 3.4a: Frequency-dependency of calibration factor, estimated from GB time series with window size of 200 data points. The mean in the range 0.8-1.2 cpd is 733.39 nm/s2/volt (STD = 0.47) and in the range 1.8 to 2.2 cpd is 735.15 nm/s2/volt (STD = 0.64).

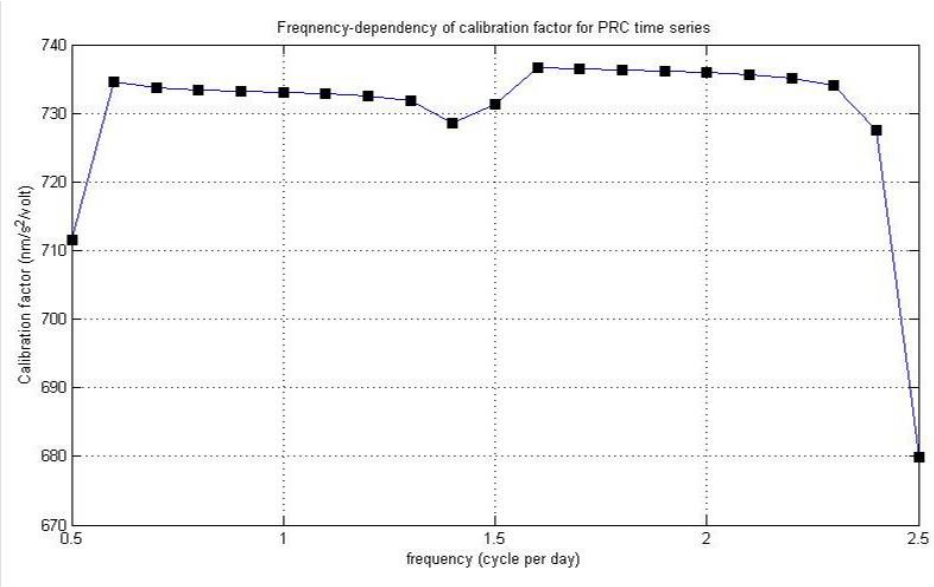

Figure 3.4b: Frequency-dependency of calibration factor, estimated from the PRC series with a window size of 200 points. The mean in the range 0.8-1.2 cpd is 733.02 nm/s2/volt (STD = 0.38) and in the range 1.8 to 2.2 cpd is 735.85 nm/s2/volt (STD = 0.46).

The calibration adopted here is 734.1 nm/s^2/volt. Uncertainty in the calibration factor is much less than 1 percent, which implies a corresponding uncertainty in hydrologic applications (e.g., measuring effects of groundwater level change). Again, this would not be a significant element of uncertainty associated with a hydrologic experiment.

The most complete Earth tide prediction model is the Wahr-Dehant-Defraigne (WDD) model (Dehant et al 1999). It is a global model and takes latitude, longitude, elevation and time as input. The Earth tides predicted by the WDD model are not sensitive to small variations in latitude, longitude, and elevation. For example, an elevation error of 10 meters produces variation in the diurnal and semi diurnal tides of .0001 nm/s^2, well below the precision of interest here. Some authors use other software, such as ETERNA3.4 to analyze tides and obtain a local Earth tides model (Wenzel 1996).

Figure 3.5a shows the GB time series and 3.5b the PRC time series, along with WDD predicted tides, and their differences. Residual variations are small relative to the original time series, as Earth tides accounts for about 90% of temporal gravity changes.

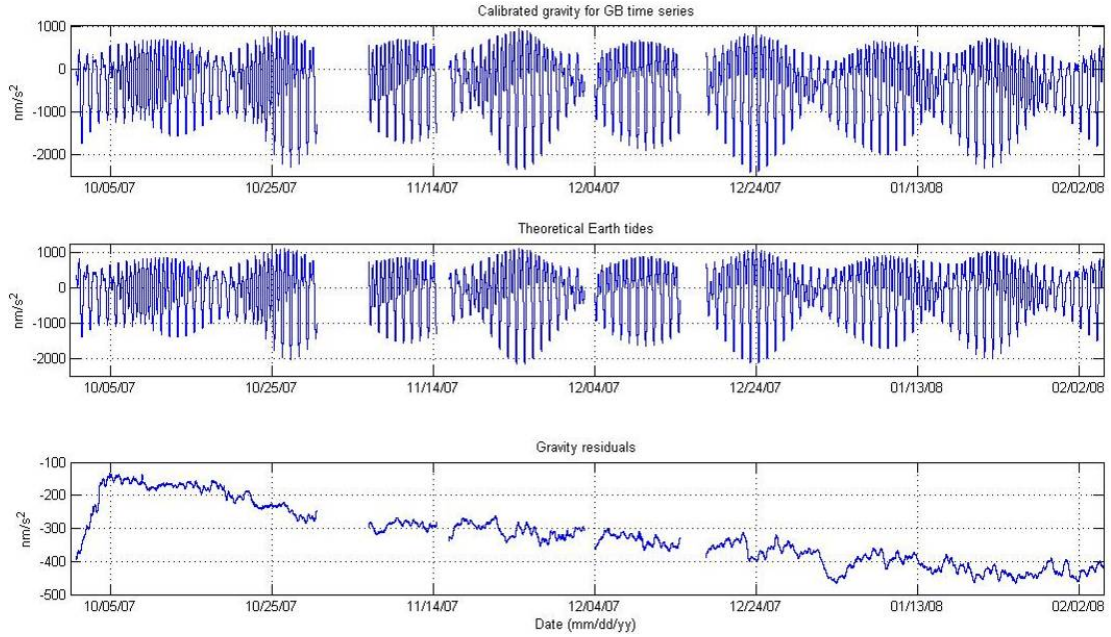

Figure 3.5a: Earth tide removal for GB time series. Top: calibrated SG data; middle: WDD Earth tides; bottom: gravity residual.

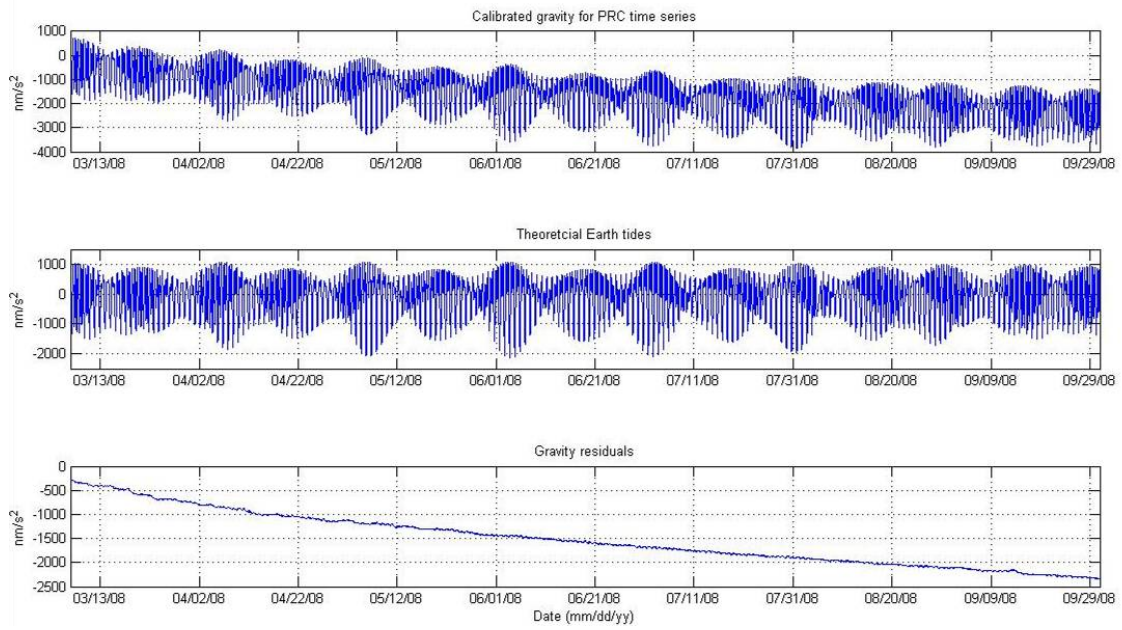

Figure 3.5b: Earth tide removal for GB time series. Top: calibrated PRC data; middle: WDD Earth tides; bottom: gravity residual.

3.2.3 Atmospheric Effects

After the Earth tides, the largest signal is the atmospheric pressure effect, which includes atmospheric mass attraction, and Earth deformation caused by pressure loading. A number of studies have examined methods to remove this effect (Spratt 1982, Van Dam and Wahr 1987, Neumeyer et. al. 2004). In any case this should be done prior to residual tidal removal because atmospheric pressure variations occur at tidal periods (once and twice per day) related to atmospheric thermal processes (Chapman and Lindzen 1970) with same periods.

The simplest way to remove the atmospheric effect is to treat the Earth as flat, and remove the attraction of an infinite slab of air mass above. The attraction of an infinite slab of air mass of horizontal extent (the Bouguer effect) is -4.3 nm/s^2 per millibar pressure change (Spratt 1982). This factor is called atmospheric admittance, and the actual value adopted in this study is less than this, around -3 nm/s^2 per millibar. A more sophisticated estimate of atmospheric attraction considers both vertical and horizontal distribution of air mass given by numerical atmospheric models. For example, Neumeyer et al (2004) use 3D atmospheric data from ECMWF or NCEP weather models to directly calculate attraction at several SG sites. The same weather data can also be used to calculate both local and globally distributed load deformation. To achieve 1 nm/s^2 precision both direct attraction and loading effects must be considered (Boy et. al. 1998). However, for purposes of hydrologic or similar studies, atmospheric effects can be removed with errors below a few percent by an empirical method. Time series of barometric pressure are regressed against observed residual gravity change to calculate atmospheric admittance. This is the approach taken in this study.

Using moving window regression in TSOFT, I estimate atmospheric admittance as a function of time. Figure 3.6a shows results for the GB time series, from October

2007 to March 2008. In each window, a linear drift is removed before fitting the admittance coefficient. Window size is 30 days, which is generally longer than typical time scales of frontal passage in Central Texas. The estimated single admittance varies from -2.3 nm/s^2/mbar to -3.1 nm/s^2/mbar, with mean of -2.82 and standard deviation (STD) of 0.20 nm/s^2/mbar. Some researches indicate that the best fit single admittance varies with the seasons (Crossley et. al. 2002). The physical explanation is that spatial scales of atmospheric pressure variations are generally different in various seasons. Varying spatial scales influence both direct attraction and loading effects. This phenomenon is shown in Figure 2.6b for the PRC time series which covers a period from Spring through Fall. In this case, a quadratic drift model is removed within each window. It shows a admittance change from near -3.0 to -4.2 nm/s^2/mbar, beginning from June 1st, and ending on July 31st. Excluding this period, the mean admittance is -2.98$\pm$0.11nm/s^2/mbar.

As in the tidal analysis, I investigate frequency-dependency of atmospheric admittance as shown in Figures 3.7a and b. At diurnal and semi-diurnal frequencies, both figures show poor correlation between gravity residual and barometric pressure. This is due to errors in Earth tides model causing small Earth tide signals to remain in gravity residuals.

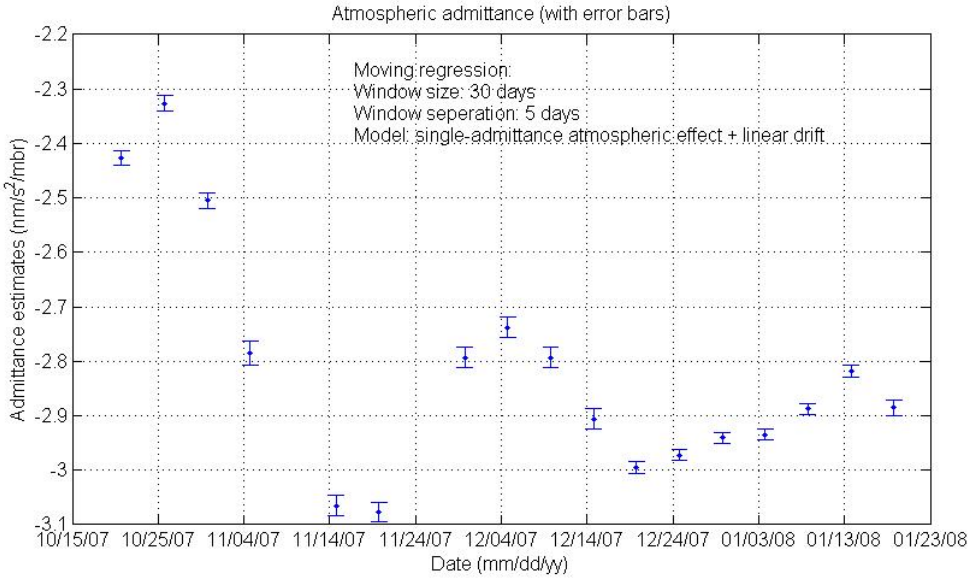

Figure 3.6a: Time-dependent variation of estimated admittance for GB time series, from October 2008 to January 2009, excluding the first week with rapid drift and portions with power-failures. The single admittance is estimated by a moving overlapping window regression of 30 days with shifts of 5 days, plus a linear drift model within each window. The mean admittance for the entire period, is -2.81 nm/s2/mbr (STD = 0.21) - a simple mean of all values, and -2.82 nm/s2/mbar (STD = 0.20) - a weighted mean where the weights are reciprocal variances of estimates.

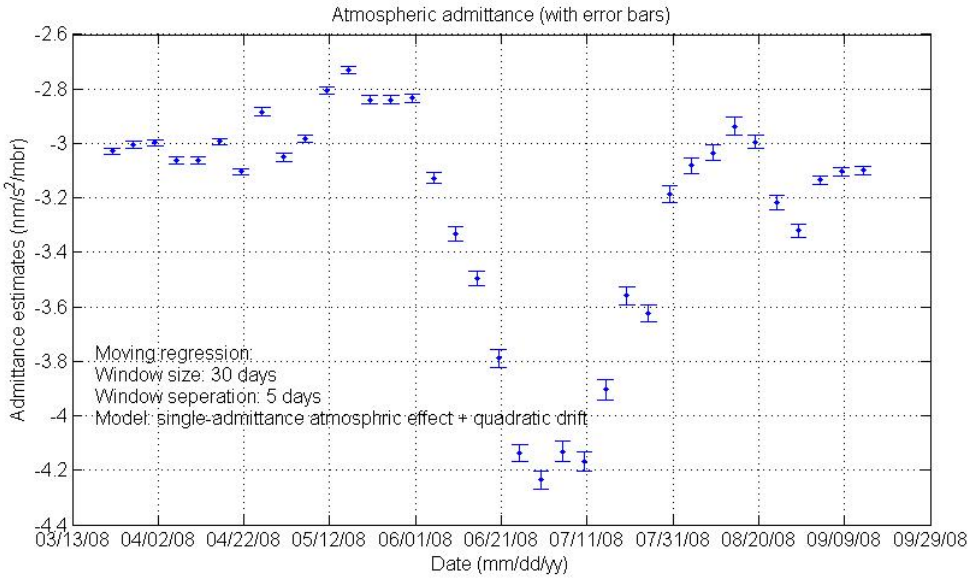

Figure 3.6b: Time-dependent variation of estimated atmospheric admittance (with error bars) for PRC time series, April-October 2008, from moving overlapping window regression of 30 days with shifts of 5 days, after removing a quadratic drift model within each window. Excluding summer (June to August), the mean admittance for the entire period, is -2.97 nm/s2/mbr (STD = 0.12) - a simple mean of all values, and -2.98 nm/s2/volt (STD = 0.11) - a weighted mean where the weights are reciprocal variances of estimates.

In Figure 3.6b, besides the higher admittance estimates, It also can see larger estimation errors in the summer period. This is expected because there is a lower variance of atmospheric pressure in summer months, causing the admittance estimate to be more uncertain. In figure 3.8, I analyze spring and summer PRC time series separately, plotting root mean square residual (RMS) for trial values of admittance over a range from -8.0 to 4.0 nm/s^2/millibar. Figure 3.9 confirms the lower variance of summer barometric pressure fluctuations. The flatter shape for summer RMS residuals corresponds to greater uncertainty in the least squares estimate of the admittance. The quadratic shape of the RMS is the basis of error bars in figure 3.6a and b.

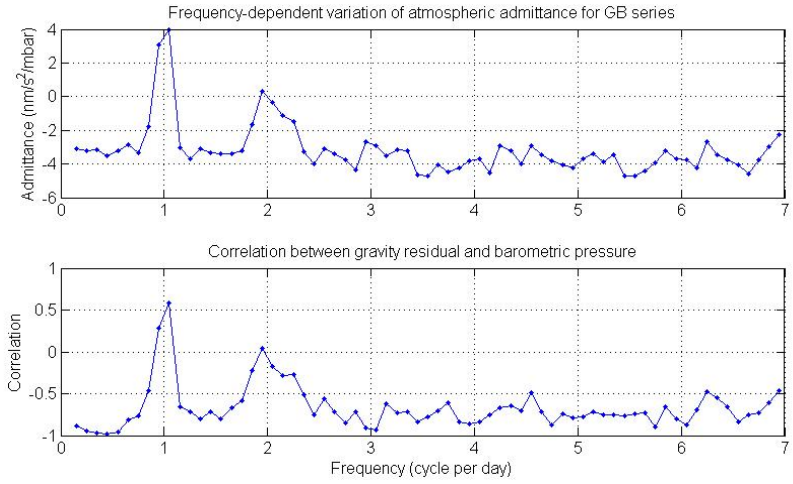

Figure 3.7a: Frequency-dependence of atmospheric admittance, estimated from GB time series using FFT band-pass filter with band width of 0.1 cycles per day (cpd). The top panel is the admittance variation. The mean in the range 2.5-7 cpd is -3.72 nm/s2/millibar (STD = 0.61) and in the range 0.1 to 0.5 cpd is -3.24 nm/s2/millibar (STD = 0.19). The bottom panel shows poor correlation at diurnal and semi-diurnal frequencies due to Earth tides remains.

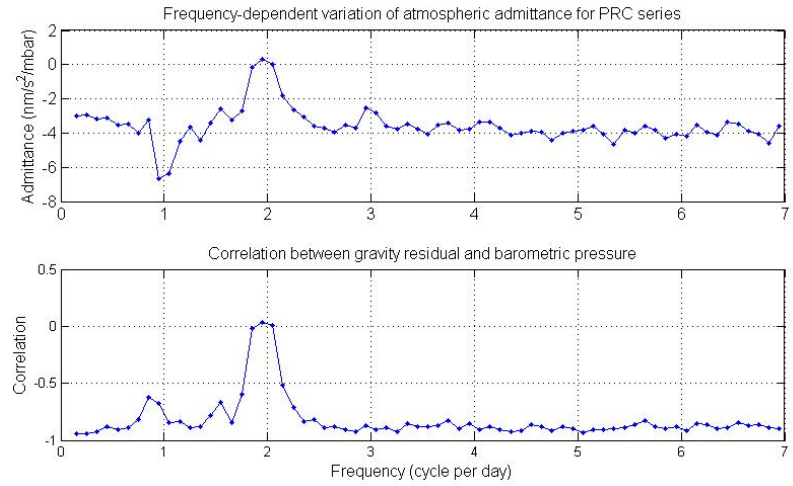

Figure 3.7b: Frequency-dependence of atmospheric admittance, estimated from PRC time series using FFT band-pass filter with band width of 0.1 cpd. The top panel is the admittance variation. The mean in the range 2.5-7 cpd is -3.70 nm/s2/volt (STD = 0.39) and in the range 0.1 to 0.5 cpd is -3.01 nm/s2/volt (STD = 0.11). The bottom panel is correlation between gravity residual and barometric pressure. It shows poor correlations at diurnal and semi-diurnal frequencies due to Earth tides remains.

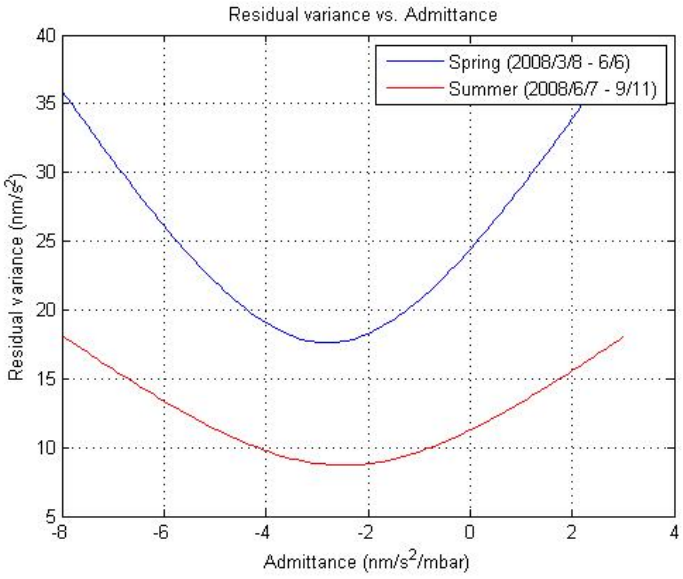

Figure 3.8: Root mean square (RMS) of gravity residual variations for spring and summer PRC series as a function of trial values of admittance. The least squares estimate is the value where this is a minimum, and uncertainty is greater for a flatter curve, in this case the summer curve (red).

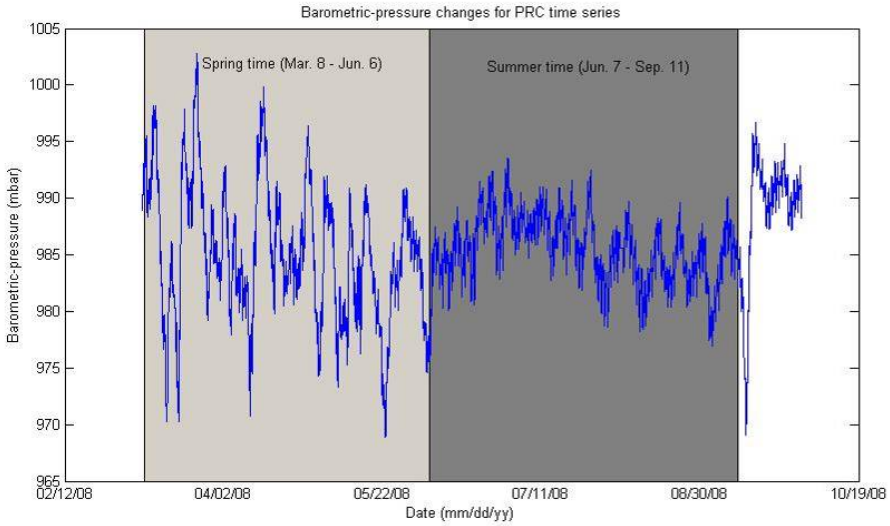

Figure 3.9: Barometric-pressure for PRC time series. Spring series, from Mar 8 to Jun 6, and summer series, from June 7 to September 11, shows different variances, and corresponding uncertainties in admittance estimates. Larger variance (Spring) leads to a better estimate because the input signal (atmospheric pressure) is greater.

In our analysis, a single admittance of -2.94 nm/s^2/mbar is adopted. It is a weighted mean of admittance for GB and PRC time series. The gravity residuals for GB and PRC time series after removing atmospheric effect are shown in figures 3.10a and b.

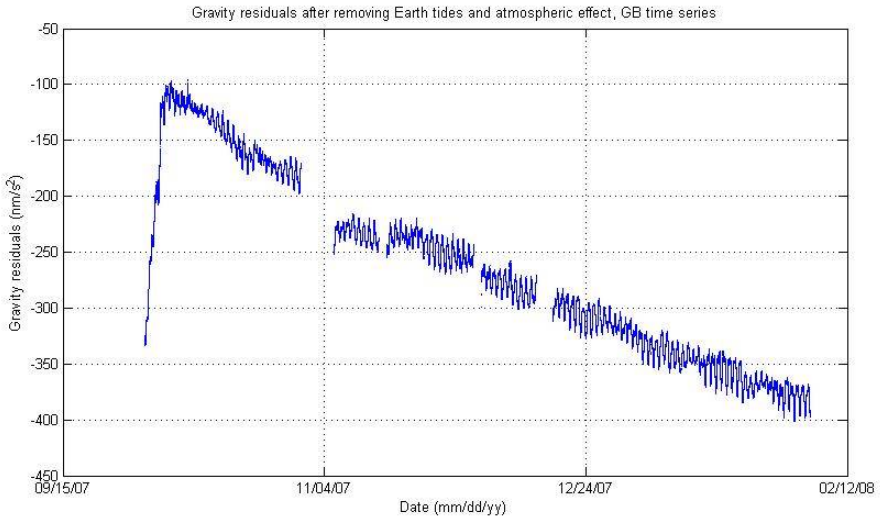

Figure 3.10a: Gravity residuals after removing Earth tides and atmospheric effect for GB time series. The atmospheric effect is calculated as: -2.94 nm/s^2/mbar * (Barometric pressure – 980.0 mbr).

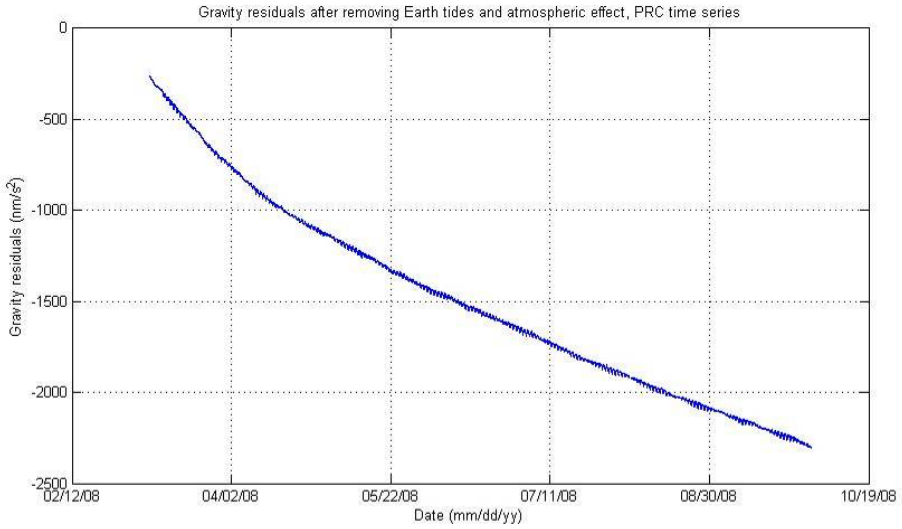

Figure 3.10b: Gravity residuals after removing Earth tides and the atmospheric effect for PRC time series. The atmospheric effect is calculated as: -2.94 nm/s^2/mbar * (Barometric pressure – 980.0 mbr).

3.3.4 Instrument drift

In figure 3.10a and b, there is evidence of instrument drifts in the gravity residual, due to imperfections of the gravity sensor. The drift is well outside the manufacturer's specifications, and was eventually repaired in the latter half of 2009 when the sensor was rebuilt at the factory. The beginning gravity increase in figure 3.10a is believed to be due to a setup error. Here I use the PRC times series for estimation of instrument drift, and residual tides. In figure 3.10b, PRC gravity residual is modeled as an exponential drift, which can be described as $A+B*exp(-t/T)$, where t is days since beginning, A is a constant, delay T and magnitude B are two parameters need to be estimated. This model is non-linear, so a minimum STD (standard deviation) is searched for to estimate parameters. As shown in Figure 3.11, the STD reaches a minimum when delay T equal to 58 days. After delay T is determined, magnitude B can be easily found using a standard linear LSQ (least square) algorithm, giving B = 1271.2 nm/s^2.

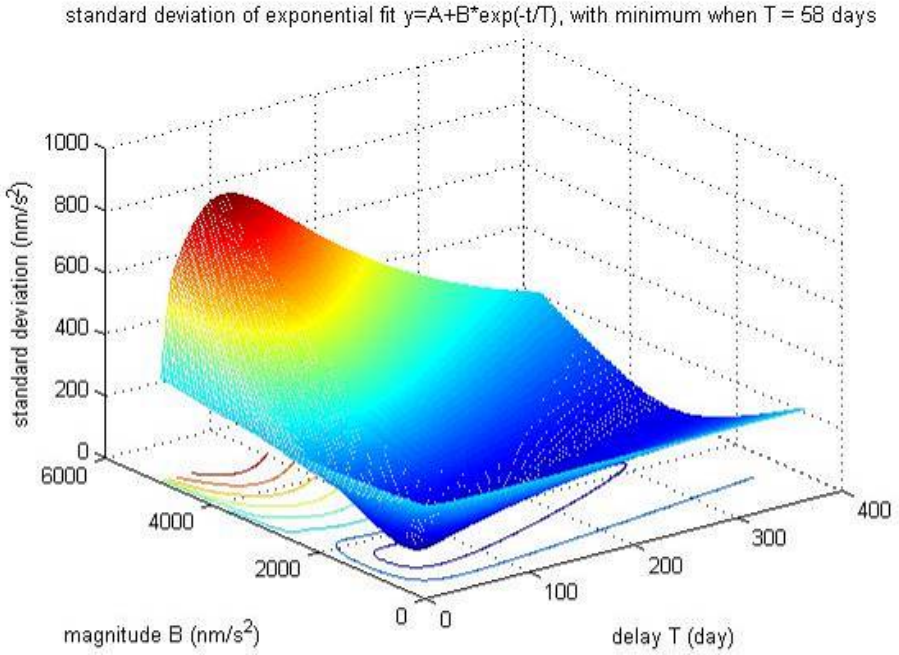

Figure 3.11: Standard deviation analysis for exponential instrument drift, *A+B*exp(-t/T)*, with delay *T* from 1 to 365 days, and magnitude *B* from 50 to 5000 nm/s^2. It has a minimum when T=58 days and B=1271.2 nm/s^2 (*A*=-729.3 nm/s^2).

I get calculate drift rate, *dg/dt=B*exp(-t/T)*(-1/T),* from 65.8 uGal per month at start (t=0 days) to 1.4 uGal per month at end (t=225 days). These values are larger than manufacturer's specified value, < 1 uGal per month, which required eventual re-build of the sensor starting in late summer 2009.

3.3.5 Residual tides

Figure 3.12 shows that tidal variations remain in gravity residual after the Earth tides, atmospheric effect and instrument drift removed. Residual tides are attributed to ocean loading effect (both globally and locally in the Gulf of Mexico), as shown in Figure 3.12. A small part might be due to errors in Earth tides model, calibration factor and atmospheric admittance. But there are sufficient differences that the ocean loading model cannot be simply subtracted. Instead, I use a residual tides model local to the Austin area, which is described in Appendix A.

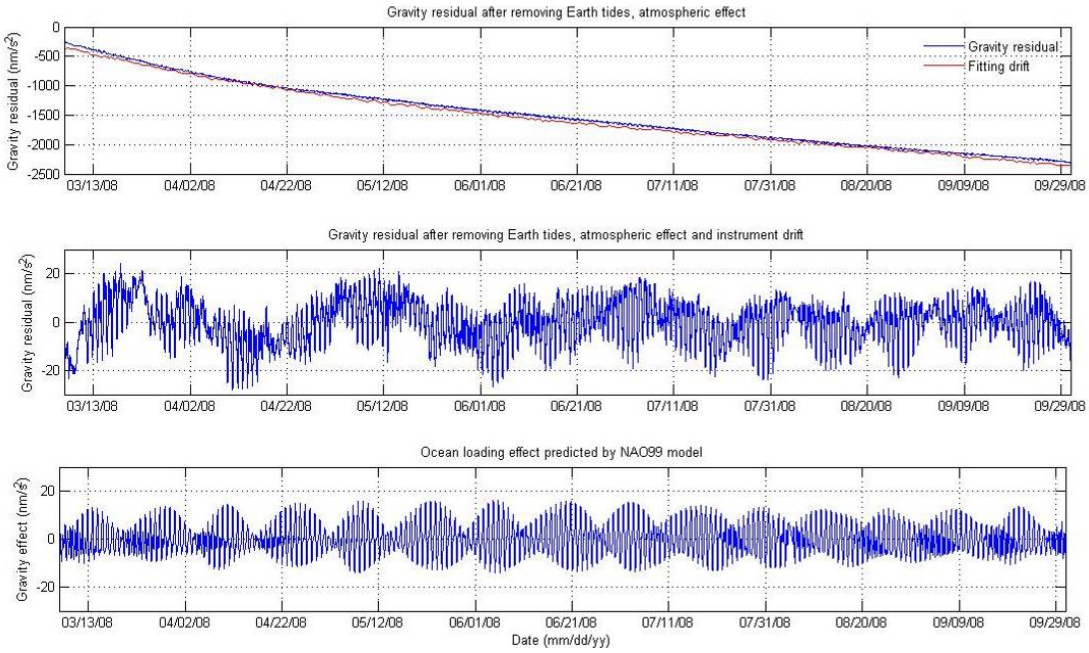

Figure 3.12: Observed tide residuals and predicted ocean loading effect for PRC time series. Top: Gravity residuals after removing Earth tides and atmospheric effect (blue), and a best-fit exponential drift (red). Middle: Gravity residual after removing the drift. Bottom: Ocean loading effect predicted by TSOFT from the NAO99 model.

Chapter 4: Operation over the Edwards Aquifer

The first field deployment of gravimeter SGo047 was intended to study the Edwards aquifer, a karst aquifer system that provides water resources in Central Texas. The purpose of the experiment was to verify SG's operability in field conditions, and its utility in groundwater storage parameter evaluation. This chapter includes an overview of the Edwards aquifer experiment, SG data overview and processing, and preliminary results.

4.1 THE EDWARDS AQUIFER

The Edwards aquifer in south central Texas is one of the largest and most important karst aquifer systems in the United States. It covers approximately 4,350 square miles (11,266.45 km^2), forming a narrow belt extending from Kinney County in the west through San Antonio area northeast to Bell County, as shown in Figure 4.1. Historically, the major towns of Salado, Georgetown, Austin, San Marcos, New Braunfels, San Antonio, Uvalde, and Del Rio were developed around large springs that flow from the aquifer.

The Edwards aquifer is contained within the Cretaceous Edwards Group limestone and associated units. It is generally covered by the Del Rio Clay and lies above the Glen Rose Limestone. The aquifer's thickness ranges from 75 to 200 m. Along the northern boundary, a series of faults in the Balcones Fault Zone has exposed the Edwards at the surface. The boundary along the south and east is the bad-water line, with water to the south and east being too salty for drinking.

Recharge to the Edwards aquifer is mainly downward percolation of surface water from streams drainage off the Edwards Plateau to the northern and west and by direct infiltration on the outcrop. Water in the aquifer generally flows from the recharge zone

towards natural discharge points such as Comal, San Marcos, Barton, and Salado Springs. Water is also discharged from hundreds of pumping wells, particularly municipal supply wells in the San Antonio region and irrigation wells in the west.

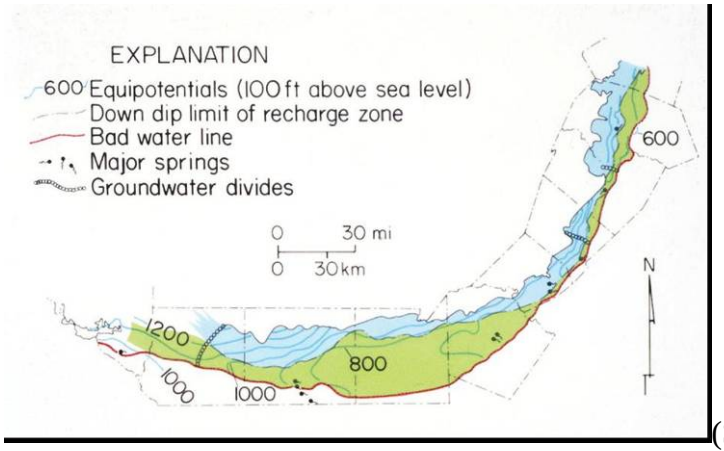

(Sharp 1997)

Figure 4.1: The Edwards aquifer (BFZ) in south central Texas. The aquifer covers parts of 11 counties, extending Kinney County in the west through the San Antonio area northeast to Bell County. The boundary along the north and west is where the rocks have been eroded. The boundary along the south and east is the bad-water line. The blue area indicates outcrop (where the water-bearing rock unit exposed at the land surface), and the green area indicates subcrop (where the water-bearing rock unit existing below other rock units).

The Edwards aquifer is one of the most productive groundwater systems in the United States with high capacity water wells and high spring discharge rates. Many locations show high (cavernous) porosity and permeability so that it responds quickly to rainfall (recharge) events. This is indicated by rapid water-level fluctuations during relative short periods of time. Under conditions of below-average rainfall or drought when discharge exceeds recharge, spring flow maybe reduced and mandatory rationing may be established (Maclay et. al 1986, Baket et. al. 1986, Sharp and Banner 1997).

4.2 TIME SERIES OVERVIEW

I chose the SG experiment site according to the following criteria. It must have an observation well to measure water level changes. It must have wired electricity service and wireless telephone service. The location must be remote from human access and other disturbing sources such as roads. The Green Emerald Terrace in south Austin meets all requirements. It is located within a former cattle ranch purchased by the City of Austin as a recharge zone for the Edwards aquifer, about 15 miles from the UT Austin main campus. Figure 4.2 shows it is in the central part of the recharge zone of the Barton Spring segment of the Edwards aquifer.

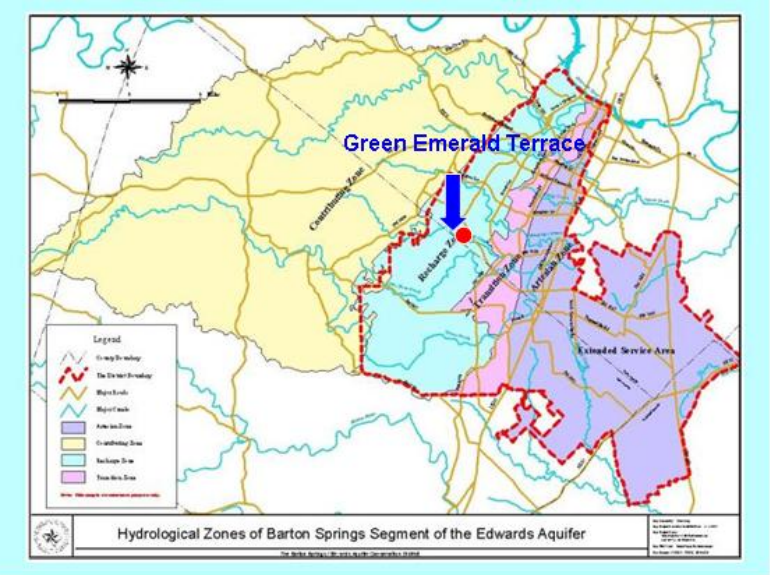

(Barton Spring/Edwards Aquifer Conservation District, 2007)

Figure 4.2: SG location on hydrological zones of the Barton Spring segment of the Edwards aquifer. Different color indicates: yellow - contribution zone, blue - recharge zone, pink – transition zone, purple – artesian zone

Three types of data were collected at the Green Emerald Terrace site: gravity data by gravimeter SGo047; water level data by the observation well and weather data by our field weather station. All data were collected from Nov. 1, 2008, when the SGo047 set

up in the field, to Jun. 14, 2009, when the SGo047 removed. The observation well was about 3 meters from the SG monument, and the weather station was set up about 10 meters away.

The original one-minute gravity data are shown in Figure 4.3, total 225 days. Due to variety of reasons, some observations have noise or other problems, and thus needed to be excluded. Three major disturbances happened in this period. One was a tilt problem during Mar. 13 ~ 15, 2009. Rainfall during that period wetted near-surface fractures filled with expansive clays, causing the gravity meter pillars to tilt. The associated tilt balance in auxiliary data is shown in Figure 4.4.

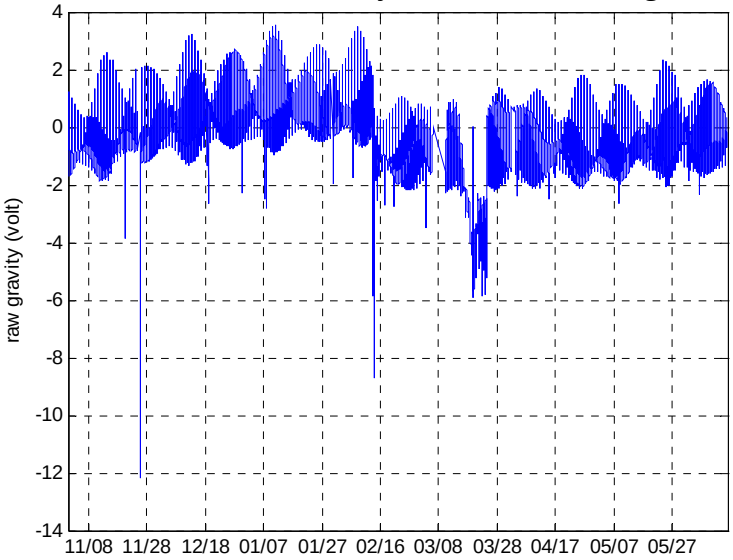

Figure 4.3: SG time series for the Edwards aquifer, from Nov.1, 2008 to Jun. 14, 2009.

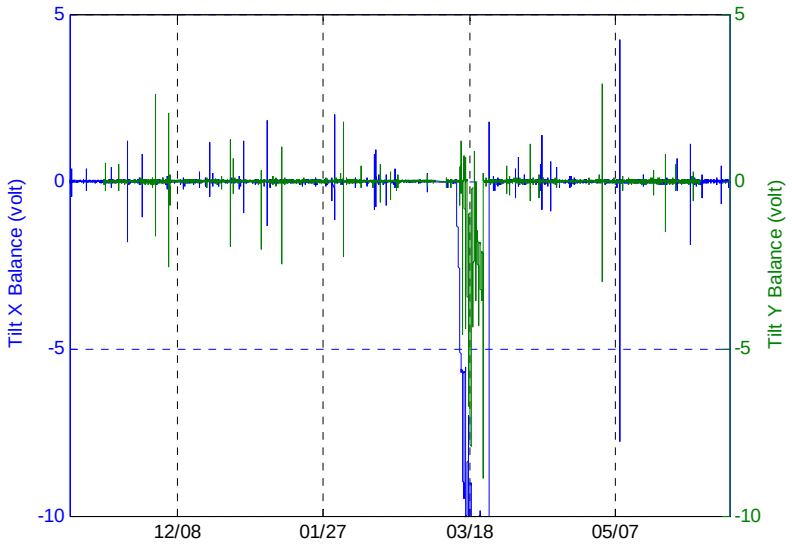

Figure 4.4: Tilt X and Y balance during heavy rain event from Mar. 13 to 15, 2009.

A second type of disturbance was contact between the dewar neck and its supporting frame, which happened during Nov. 10 ~ 25, 2008 and May 9 ~ Jun. 14, 2009. The SG dewar stands on pillars cemented into to the limestone, but the supporting frame rests on the shed floor. The shed floor was made of plastic over plywood, and deformed with heavy loads, causing the frame to contact the gravity meter dewar. Figure 4.5 shows tilt powers and SG neck temperature. Great periodic noise in tilt powers and neck temperature is a sign of such contact. Fixing this problem required a visit to the site to adjust the level screws on the dewar frame.

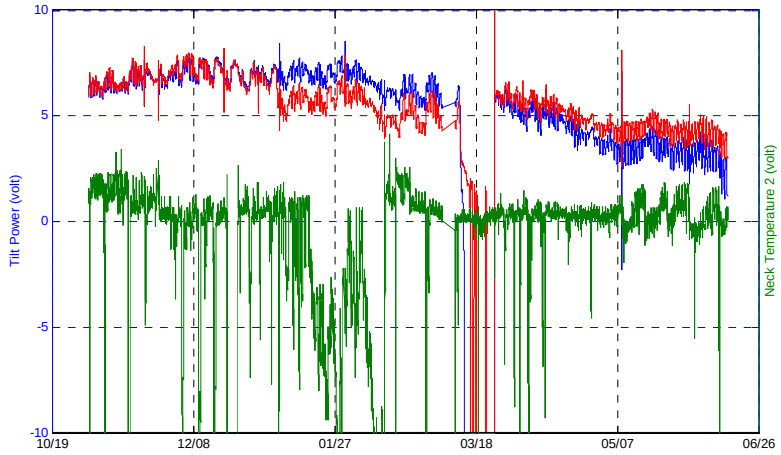

Figure 4.5: Tilt power and dewar neck temperature in dewar contact events, happened during Nov. 10 ~ 25, 2008 and May 9 ~ Jun. 14, 2009.

The third type of event was refrigerator malfunction, which happened during Dec. 20 ~ 24, 2008 and Jan. 9 ~ Feb. 15, 2009. In first instance, the data system and electronics power remained on, but the compressor and cold-head were not working. In the second case, the compressor and cold head were working with low efficiency. These two events are shown by dewar pressure and neck temperature in Figure 4.6. Because a full dewar with liquid helium can hold up to 20 days without refrigeration, these two events has no effect on our gravity observation. Refrigerator efficiency was restored by purging the cold-head of impurities (frozen gas such as oxygen and nitrogen).

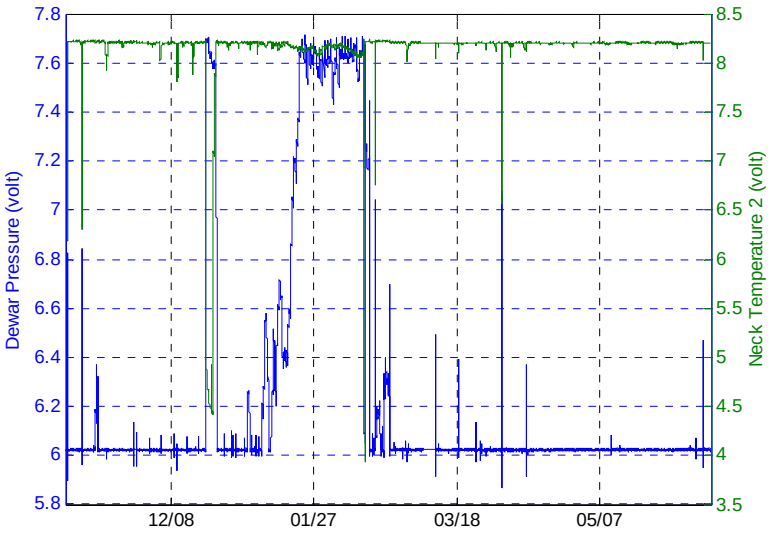

Figure 4.6: Dewar pressure and neck temperature in refrigerator malfunction event, happened during Dec. 20 ~ 24, 2008 and Jan. 9 ~ Feb. 15, 2009.

Other spikes, gaps and steps in Figure 4.1 may come from brief power failures, and road constructions near the site. In Figure 4.7, gravity observations with great noise have been excluded. Spikes and steps were corrected as I did in Chapter 3 using TSOFT.

4.3 DATA PROCESSING

According to the standard data processing described in chapter 3, most known gravity effects including Earth tides, atmospheric effect and residual tides (including tidal model deficiencies and oceanic loading effects) can be modeled and removed from gravity observations. The residual is shown in Figure 4.8. A calibration factor, 734.1 nm/s2/volt, WDD Earth tides model and single atmospheric admittance, -2.94 nm/s2/mbar was applied here. The residual tides model was obtained from PRC time series (see Appendix A).

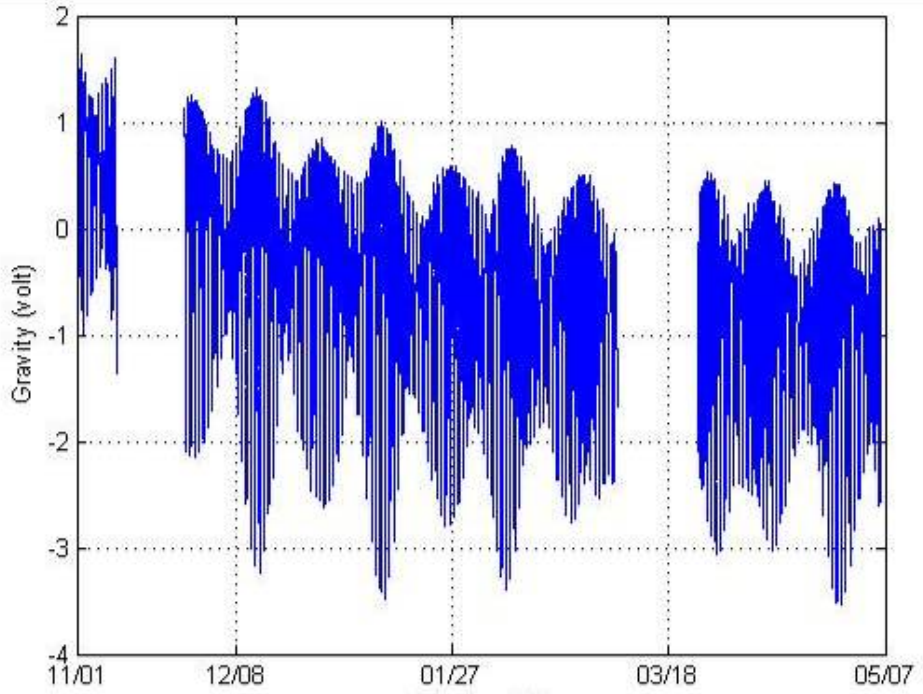

Figure 4.7: Preconditioned SG time series for the Edwards aquifer.

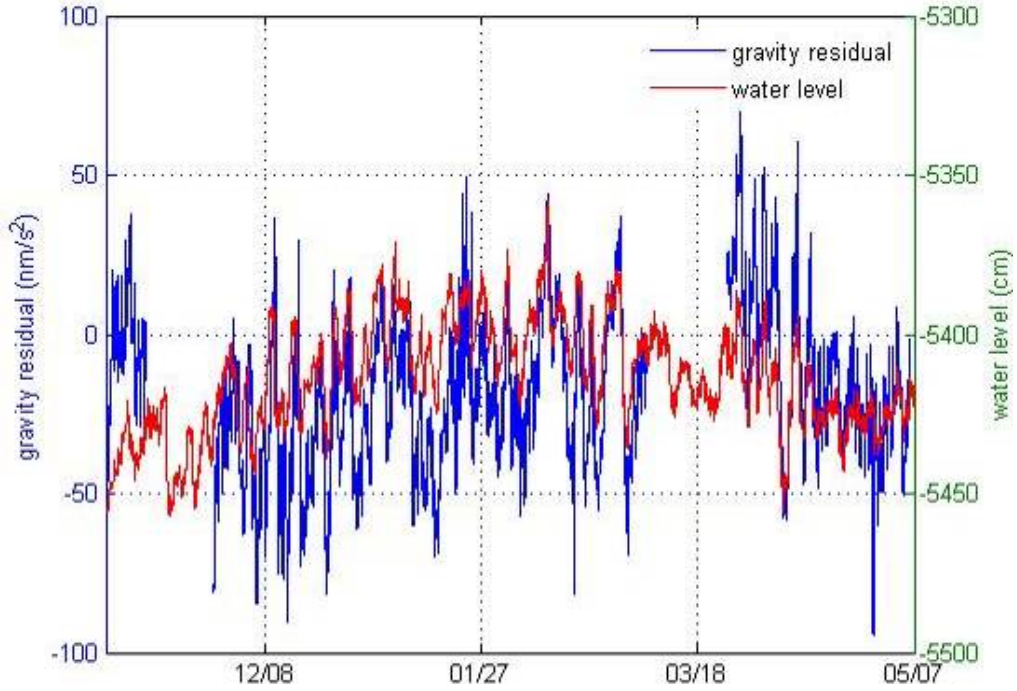

Figure 4.8: SG gravity residual and water level changes for the Edwards aquifer. Earth tides, atmospheric effect, instrument drift, and residual tides have been removed from gravity.

4.4. PRELIMINARY RESULTS

On SG site, there was a borehole for water level observation. It was equipped with a vented transducer, Level Troll 500, to measure water temperature and pressure in psi. The pressure can be converted into level depth to water in feet, which is the negative of water level changes. The reference water level is 179.53 ft (54.72 m), and the depth of probe is 40.71 ft (12.4 m). The well observation was sampled every 15 minutes. I plot it with SG gravity residual in figure 3.5. It's clear that there are correlations between the two signals. However, subsequent study showed that both gravity and well level changes are highly correlated with barometric pressure. In fact most of the well level changes in this period were caused by barometric pressure forcing, because the period November 2008-June 2009 was one of exceptional drought in Central Texas. It is well known that an increase in barometric pressure typically causes a decrease in well level, an effect described by a parameter called barometric efficiency. For example, a barometric efficiency of 1 implies that one mbar of air pressure increase will cause water level to decrease by one cm, as a consequence of forcing water away from the vicinity of the well bore. More detailed subsequent analysis showed that the barometric efficiency of the Green Emerald Terrace well is about 1.9 at periods of a week or less, decreasing to about 1.0 at periods longer than 20 days. Similarly, gravity responds to barometric pressure, as described earlier, causing a decrease in gravity by about 2.9 nm/sec^2 (or 0.29 μGal) per mbar increase in winter months in Austin. Thus, common forcing by barometric pressure introduces a correlation between gravity change Δg and water level ΔH that has exactly the same sign as equation 1.2 which is repeated here:

$$\Delta g = 41.92 S_y \Delta H \qquad \mu Gal / m \tag{4.1}$$

In the absence of changes in stored water in the aquifer, a 1 mbar increase in barometric pressure at Green Emerald Terrace produces about 0.29 μGal gravity decrease, and 0.019 m water level decrease. Thus an apparent value of S_y would be [(0.29)/(0.019)]/(41.92) = 0.364 or about 36%. To avoid this problem, it is essential to remove from both gravity and water level any signal that is related to barometric pressure. This task is beyond the scope of this thesis, and is not simple to accomplish because barometric efficiency is found to be a function of frequency. (Wilson et al, 2011)

Chapter 5: Conclusion

To summarize the results of this study:

1. With development of a compact refrigerator system, a superconducting gravimeter has been configured as a field instrument, which can be easily deployed in the field and transported between observation sites, with remote control and data transfer. The high-quality measurements on gravity changes make it possible to evaluate ground water changes equivalent to a one centimeter layer of water.
2. With the help of software, TSOFT, a standard procedure was developed to process SG gravity data, including data preconditioning and calibration, Earth tides calculation, atmospheric effect estimation, instrument drift removal, residual tides modeling. The residual gravity is due to changes in stored water beneath the gravimeter.
3. The first transport and field tests have confirmed the system's capacity to observe gravity change in the field with high quality, and verified procedures for instrument transport, site preparation, and SG setup.
4. In field operations at the Edwards aquifer, preliminary result shows correlations between residual gravity changes and groundwater (water level) changes. Further analysis will be required to remove atmospheric effect from both signals, so that specific yield of the aquifer can be estimated.

Appendix A: Explanation of Residual Tides Model for Austin, TX

For all bodies of the universe moving in a stationary orbit (e.g. the Earth), the gravitational accelerations produced by other bodies (e.g. Moon, Sun) are completely compensated at their center of mass by centrifugal acceleration. Because of the spatial extent of the body (e.g. Earth), gravitational acceleration is slightly position dependent, while centrifugal acceleration is constant within the body and on the surface of the body. The difference between gravitational acceleration and centrifugal acceleration is called tidal acceleration, and is observed to vary in time as the Earth rotates. On Earth, the tidal accelerations are less than ± 1 μm/s^2 = 10^{-7} of the Earth gravity g.

Tidal acceleration, as well as tidal tilt and tidal strain are functions of the tidal potential, which can be expanded in spherical harmonics as in the following (excluding Earth's flattening effects):

$$V = \frac{GM_b}{s}\sum_{l=2}^{\infty}\left(\frac{r}{s}\right)^l \frac{1}{(2l+1)}\sum_{m=0}^{l}\overline{P}_{l,m}(\cos\theta)\cdot\overline{P}_{n,m}(\cos\Theta_b)\cdot\cos(m\lambda - m\Lambda_b) \qquad \text{(A.1)}$$

where $\overline{P}_{l,m}$ are fully normalized spherical harmonics with l = degree, m = order; M_b is mass of the celestial body; r, λ, θ are geocentric radius, longitude and co-latitude of the station; s, Λ_b, Θ_b are geocentric distance, longitude and co-latitude of the celestial body, they are time-dependent because of the Earth rotation, and orbital movements of Earth and Moon.

In eqation A.1, the geocentric longitude Λ_b of the celestial body is multiplied by spherical harmonics order m. Because the geocentric longitude Λ_b varies by about 2π per 24 hours due to Earth rotation, the tidal potential of a certain degree varies at a certain station for:

m = 0: with periods of 14 days to 18.6 years, called long periodic waves

m = 1: with periods about 24 hours, called diurnal waves

m = 2: with periods about 12 hours, called semidiurnal waves

m = 3: with periods about 8 hours, called terdiurnal waves

…

Spectral analysis of the tidal potential's spherical harmonic expansion yields a tidal potential catalogue (a table of amplitudes, phases and frequencies for tidal waves), as shown in Table A.1. Using such tidal catalogues and additional information of Earth elasticity and ocean tides, tidal acceleration can be computed.

Tidal acceleration tends to deform the Earth. The largest phenomenon which presents the Earth's response to the lunar-solar tidal force is the ocean tide (rising of Earth's ocean surface caused by tidal forces acting on the oceans), but also there are deformations of the solid Earth, called body tides. In addition to tidal body forces, surface forces from the pressure of the ocean tide act on the Earth, and deform it, creating the load tides. While the body tide varies smoothly over the earth surface, the load tide is more irregular because of the discontinuity in the force function at the coastline and localized loading within oceanic basins, seas and bays.

Over the past several decades great progress has been made in computing deformations for realistic Earth models (e.g. Longman 1962, 1963 and Farrell 1972). The theoretical tidal parameters (Love numbers) describing effects of Earth deformation agree very well with observations. The current difference between observations and theory is on the level of a few percent (Wilhelm et al 1997). In this thesis, we study the gravity variations at a certain station on Earth's surface. In order to retrieve a gravity signal caused by water storage changes, we must remove tides from the data record, so that residual tide variations are below the level of the signal of interest, about 1 microgal.

The solid body tide, including solar-lunar tides acting on Earth and Earth deformation response to it, are well modeled by the current WDD model (Dehant, Defraigne, Wahr 1997), widely regarded as the best available. But for ocean loading effects, predictions from ocean tide models are imperfect (especially for stations close to the ocean, like Austin, Texas). To remove tidal effects at the 1 microgal level, we must therefore subtract the standard WDD model from the observed gravity data, and then fit a residual tide model to observations at a particular location, in this case Austin, Texas.

The following describes how to get this residual tide model, using observations taken with the SG in the Austin area. As seen in chapter 3 and figure 3.12, after removing Earth tides and atmospheric effect, there are clear tidal variations remaining in gravity residuals for the PRC time series. To achieve microgal-level gravity residuals associated with hydrological activity, it is vital to remove those tidal residuals. Our solution is to get a residual tide model using tidal analysis in TSOFT. From computations in TSOFT, we can show that the gradient of the tidal variations due to the load tide are on the order of 10^{-4} microgal per km (North-South, approximately in the direction towards the nearest ocean in the Gulf of Mexico). Therefore, this tidal model should be accurate for all our experimental sites, including the Geology Building (GB) in UT campus and Pickle Research Campus (PRC), and the Edwards aquifer (EA) site. To test the tide model, we obtain it from the PRC time series, then apply it to both PRC and GB time series.

The PRC time series has a length of about one-half year, from April to October, 2008 with a sampling rate of 1 minute. We fit a residual tide model with 18 components (as shown in Table A.1, including diurnal, semidiurnal and terdiurnal waves plus lunar waves of 13.66 days) to its gravity residuals after removing WDD solid Earth tides and atmospheric effects. All procedures are done in the software package TSOFT. At

first, we use menu option <Location|Add location> to add the site PRC (with longitude, latitude and height) into the database, then use <Theotide|Compute tidal parameters> to compute solid Earth tides (as in Table A.1) by the WDD model. After that, we select this WDD tide and use <Theotide|Calculate> to calculate the Earth tide time series. Atmospheric effects are removed according to Chapter 3. This leaves the residual gravity variation on which we use <Tide|Fit Tidal model> to perform a tidal analysis and obtain the residual tide model. This model can be used to calculate residual tides for any location within the Austin area, just as calculation of solid Earth tides using the command <Theotide|Calculate>.

More details on the full data processing procedures and results are described in Chapter 3. As shown in Figure A.1, the residual tide model removes virtually all diurnal and semi-diurnal waves in PRC time series, and leaves only seasonal variation at the microgal level. Table A.1 gives the wave groups of the residual tide model, showing largest components at diurnal and semi-diurnal frequencies. Figure A.2 shows its comparison with ocean loading effect predicted by a standard ocean tide model, NAO99 contained in ETERNA3.4 (an Earth tide data processing package). They are of similar size, though different in detail, confirming that the residual tide model computed from the data is almost certain to be an ocean loading effect. Figure A.3 shows application of the residual tide model computed from the PRC series to the GB time series. The result is likewise successful, confirming its utility to remove residual tidal variations for Austin area data.

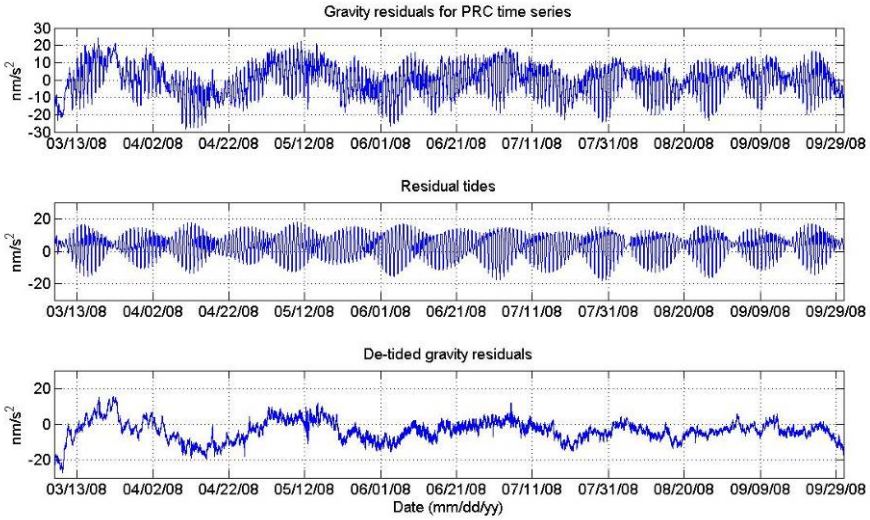

Figure A.1: Residual tide model for Austin Texas, obtained from the PRC time series. Top: Gravity residuals after removing Earth tides, atmospheric effects and instrument drift. Middle: Residual tide model obtained from gravity residuals, with wave groups shown in Table 2.1. Bottom: Gravity residuals after removing residual tides. This represents the signal of interest in hydrologic and other applications.

Min Freq. (cpd)	Max Freq. (cpd)	Amplitude factor (δ)	Phase shift (deg.)	Group name
Earth tide model				
0.000000	0.002427	1.00000	0.0000	Long
0.002428	0.249951	1.15800	0.0000	Mf
0.721500	0.906315	1.15437	0.0000	Q1
0.921941	0.940487	1.15435	0.0000	O1
0.958085	0.998028	1.14901	0.0000	P1
0.999853	1.003651	1.13412	0.0000	K1
1.005329	1.005623	1.27502	0.0000	PSI1
1.007595	1.01109	1.17110	0.0000	PHI1
1.013689	1.216397	1.15645	0.0000	OO1
1.719381	2.182843	1.16208	0.0000	All2
2.753244	3.381478	1.07366	0.0000	M3
3.381379	4.347615	1.03900	0.0000	M4
Residual tide model				
0.000000	0.000913	0.14914	89.3919 -	long
0.002428	0.249951	0.00656	1.2264	Mf
0.748077	0.906315	0.01354	104.3083	Q1
0.921941	0.940016	0.01487	97.0023	O1
0.958086	0.974041	0.02154	104.0006	NO1
0.991787	0.997881	0.01542	101.7344	P1
1.000000	1.000000	0.42605	99.5500	S1
1.001972	1.003504	0.01611	83.6931	K1
1.005476	1.005623	0.22568	-160.8767	PSI1
1.007742	1.011099	0.05484	-61.7792	PHI1
1.013689	1.044800	0.01256	82.8067	J1
1.064841	1.216397	0.01118	86.2653	OO1
1.724238	1.872142	0.02401	-141.5142	2N2
1.888387	1.906462	0.02529	172.6338	N2
1.924679	1.942753	0.01860	133.0248	M2
1.960823	1.976926	0.06250	-72.1904	L2
1.994524	2.002738	0.03555	-89.9063	S2
2.003032	2.182696	0.03370	-79.0400	K2
2.758101	3.081254	0.00879	-176.0405	M3

Table A.1 Solid Earth tides for Pickle Research Campus, obtained by the WDD model (Wahr Dehant Defraigne 1999), and residual tide model for Austin, Texas, calculated by TSOFT from the PRC time series. Each line contains the wave group name, maximum frequency inside the group (in cycles per day), the amplitude factor (δ), the phase shift (actually phase lead, in degrees), and the name of the wave group.

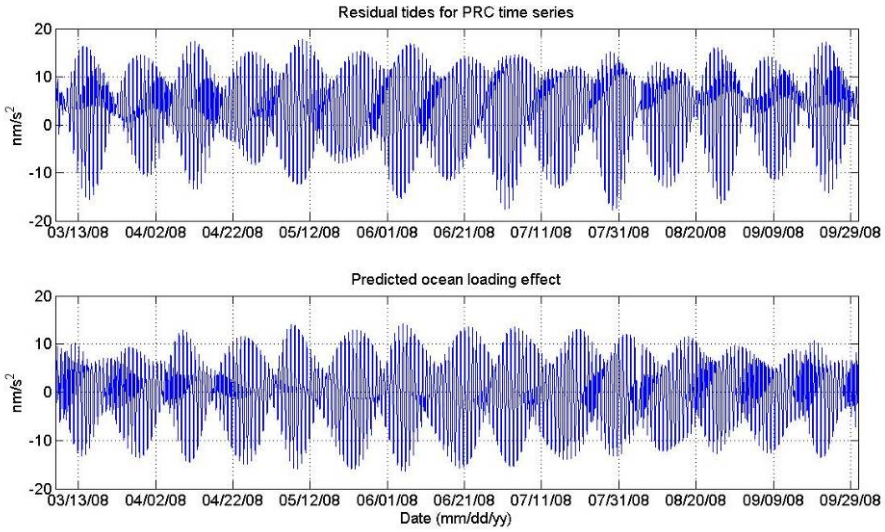

Figure A.2: Comparison between residual tide model determined from the PRC series above, and Ocean loading effect predicted by a standard ocean tide model (NAO99) model. Amplitudes are similar, confirming that the PRC-based residual tide model is most likely due to ocean loading.

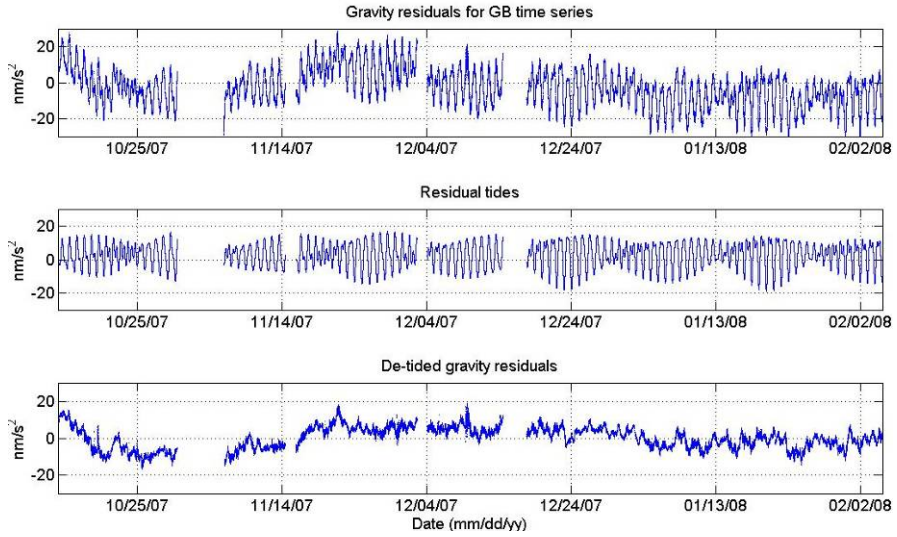

Figure A.3: Removal of residual tides for GB time series. Top: Gravity residuals after removing Earth tides, atmospheric effect. Middle: Residual tides predicted by the model for Austin Texas, obtained from PRC time series. Bottom: Gravity residuals after removing residual tides, showing the effectiveness of the residual tide model.

Appendix B: Maintenance of SGo047

The SRDK 101 cold-head, manufactured by Sumitomo Heavy Industry (SHI) Inc., has a life expectancy of more than 10,000 hours (1.1 year). During normal operation in the dewar, the cold-head often runs much longer before requiring service. The compressor maintenance schedule requires exchange of the oil absorber module at 30,000 hr (3.4 yr) intervals. The SHI compressor uses ultra high purity helium in a closed system as its working fluid. When impurities in the gas collect in the cold-head and disrupt piston movement, it can cause loud noises and impair cold-head performance. In such cases, the cold-head needs a purge procedure which has been developed by GWR.

As mentioned before, the SHI compressor can liquefy helium gas from a standard high pressure gas cylinder. GWR supplies a high pressure regulator CGA-580 that can be attached to the cylinder and used to reduce and adjust the pressure manually between 0 to 600 psi (0 to 4,136.85 kPa). This is a metal to metal seal, made by tightening the nut with an open ended wrench. The following shows the procedure to do it.

1. Turn needle valve on GWR regulator to stop air flowing into the dewar.
2. Turn GWR regulator to dead left to decrease air pressure.
3. Close cylinder's regulator valve.
4. Loose the nut with a wrench to detach GWR regulator from gas cylinder.
5. Replace the gas cylinder.
6. Attach GWR high pressure regulator and tighten the nut.
7. Open regulator valve on gas cylinder.
8. Open needle valve slowly to allow helium-gas flowing into the dewar.
9. Adjust GWR high pressure regulator to around 50 psi.

10. Watch the dewar pressure, it will rise to a stable value, and the diaphragm bulges. If it's not around the set value (e.g. around 0.1 psi/689.5 Pa), go to next step.
11. Adjust the precision low pressure regulator (attached to dewar head) slowly to increase or decrease the dewar pressure.

Appendix C: Computer settings and commands for SG system operation

Our entire SG system (including GPS receiver, weather station etc.) is managed and operated by an on-site PC computer, which can be accessed via wireless internet. The computer runs Windows XP operation system, with GWR UIPC (for SGo047 electronics), Compbellsci Loggernet (for weather station data-logger) and Verizon Access-manager (for wireless internet connection) software installed. It can automatically collect data and transfer to remote server; monitor its performance and notify remote users with following script codes and system setting.

C.1 REMOTE ACCESS VIA WIRELESS INTERNET.

The computer uses a USB wireless modem from Verizon to provide wireless internet connection, which is managed by program Verizon Access-manager. A third-party software RealVNC enables remote access and full control to the computer (as server) from your computer desktop (as client) across wireless internet. The software can be download from http://www.realvnc.com. The Verizon modem provides static IP address for the computer. If it's not the case, a script *chk_ip* can be used to check IP address and get users updated via email.

C.2 DATA COLLECTING AND TRANSFER SCRIPT

It's a Windows commands-line script, or called BAT file, which is scheduled to run at 12:30 am each day. The script downloads yesterday's data from GPS receiver, rename data files with date stamp, and upload them to a remote Unix server using PSFTP. All ftp commands come from a text file created by script itself. Public key authentication is used to login UNIX server.

In Windows XP control panel, choose *Scheduled Tasks*, add task *MyDailyTransfer*, which executes *start /min "C:\Program files\Campbellsci \LoggerNet\stampme.bat"*, in directory *"C:\Program files\Campbellsci\LoggerNet\"* (don't forget double quotation marks), choose user *SG-047\SG Administrator* without password (but need to check the option "Run Only if Logged on"), schedule the task as daily and start at 12:30 am.

PSFTP, part of free software PUTTY, uses SSH2 protocol to transfer data files. Firstly, a pair of keys need to generated (it's better not to using paraphrase to protect the keys). The private keys saved in local computer, the public keys uploaded to the server in subfolder *.ssh2*. A line of key index, like *key KeyFilename*, needs to be added in file *authorization*. Then, in command line of PSFTP, use –I option to specify the private key file.

```
Filename: chk_ip.bat
::@echo off
setlocal

for /f "skip=2 tokens=1 delims= " %%G IN (new_ip.txt) do set _ipaddr=%%G
for /f "tokens=2 delims=:" %%G in ('"ipconfig|find "IP Address"|find /v "192.168."""') do set
_ipaddr1=%%G

if not defined _ipaddr1 (
   ping -n 61 127.0.0.1>nul
   for /f "tokens=2 delims=:" %%G in ('"ipconfig|find "IP Address"|find /v "192.168."""') do set
_ipaddr1=%%G
   if not defined _ipaddr1 (
      taskkill /f /im "VZAccess Manager.exe" /t
      ping -n 6 127.0.0.1>nul
      start "VZAccess Manager" /d "C:\PROGRA~1\VERIZO~1\VZACCE~1" "C:\Program
Files\Verizon Wireless\VZAccess Manager\VZAccess Manager.exe"
      ping -n 61 127.0.0.1>nul
      for /f "tokens=2 delims=:" %%G in ('"ipconfig|find "IP Address"|find /v "192.168."""') do set
_ipaddr1=%%G
   )
)

if not %_ipaddr1: =%==%_ipaddr: =% (
   date /t >new_ip.txt
   time /t >>new_ip.txt
   echo %_ipaddr1: =% >>new_ip.txt

   sendemail -f sgo47@gmail.com -t wuhongqiu@mail.utexas.edu crwilson@mail.utexas.edu
laurent.longuevergne@beg.utexas.edu -s smtp.gmail.com:587 -u "SGo047 IP Address" -o message-
file="new_ip.txt" -xu sgo047@gmail.com -xp gravity047
)
```

File name: stampme.bat
Directory: C:\program files\Campbellsci\LoggerNet

```
::@ECHO off
SETLOCAL

FOR /f "tokens=2-4 delims=/ " %%G IN ('date /t') DO (
        SET _mm=%%G
        SET _dd=%%H
        SET _yy=%%I
)

call datemath %_yy% %_mm% %_dd% - 1

move /y CR23X_final_storage_1.dat "c:\program
files\campbellsci\LoggerNet\RawData\CR23X%v_ymd_str%.dat"

:: Download files from NetRS (GPS receiver)
echo open 192.168.0.40>GetGPSData.txt
echo anonymous>>GetGPSData.txt
echo anonymous>>GetGPSData.txt
echo cd %v_ymd_str:~0,6%>>GetGPSData.txt
echo cd z>>GetGPSData.txt
echo binary>>GetGPSData.txt
echo mget NetRS%v_ymd_str%??00z.T00>>GetGPSData.txt
echo quit>>GetGPSData.txt

ftp -i -s:GetGPSData.txt

move /y NetRS*.* c:\NetRS\RawData

:: Upload all files to GEO unix server
echo cd SGo047/RawData/Gravimeter>PutAllData.txt
echo lcd c:\GWR_o047\%v_ymd_str:~0,4%o047\DAY_o047>>PutAllData.txt
echo mput ??%v_ymd_str:~2%.zip>>PutAllData.txt
echo cd ../NetRS>>PutAllData.txt
echo lcd c:\NetRS\RawData>>PutAllData.txt
echo mput NetRS%v_ymd_str%??00z.T00>>PutAllData.txt
echo cd ../WeatherStation>>PutAllData.txt
echo lcd "c:\Program files\Campbellsci\LoggerNet\RawData">>PutAllData.txt
echo put CR23X%v_ymd_str%.dat>>PutAllData.txt
echo quit>>PutAllData.txt

"c:\program files\putty\psftp" -batch -b PutAlldata.txt -be -i mykey1_private.ppk
wuh@flute.geo.utexas.edu
```

Final name: emailperf.bat
Directory: C:\perflogs
echo %1 > mylog.txt
echo %2 >> mylog.txt
echo %3 >> mylog.txt
echo %4 >> mylog.txt
echo %5 >> mylog.txt

set _counter=%3
if "%_counter:~-15,14%"=="Processor Time" call "c:\perflogs\killtopproc.bat"

"c:\program files\campbellsci\loggernet\sendemail.exe" -f sgo47@gmail.com -t wuhongqiu@mail.utexas.edu -s smtp.gmail.com:587 -u "SGo047 Performance Alert" -o message-file="mylog.txt" -xu sgo047@gmail.com -xp gravity047

Final name:killproc.bat
Directory: C:\perflogs

```
::@echo off
setlocal

set _maxusage=0
set _topname=NULL
set _toppid=NULL

tasklist /v /fo csv /nh >p1.txt
ping -n 61 127.0.0.1>nul
tasklist /v /fo csv /nh >p2.txt

for /f "skip=1 tokens=1 delims=" %%G in (p2.txt) do (
   call :cputime %%G
)

if %_maxusage% LSS 50 (
   goto :eof
)

taskkill -f /pid %_toppid% /t

echo Top process has been killed. >>mylog.txt
echo Process Name: %_topname%    >>mylog.txt
echo PID: %_toppid%    >>mylog.txt
echo CPU usage: %_maxusage%%    >>mylog.txt

if %_topname%=="VZAccess Manager.exe" (
   ping -n 6 127.0.0.1>nul
   start "VZAccess Manager" /d "C:\PROGRA~1\VERIZO~1\VZACCE~1" "C:\Program Files\Verizon
Wireless\VZAccess Manager\VZAccess Manager.exe"
   echo VZAccess Manager has been restarted.    >>mylog.txt
)

if %_topname%=="explorer.exe" (
   ping -n 6 127.0.0.1>nul
   start /d c:\windows c:\windows\explorer.exe
   echo explorer.exe has been restarted.    >>mylog.txt
)

sc stop winvnc4
ping -n 6 127.0.0.1>nul
sc start winvnc4
echo Service "winvnc4" has been restarted.    >>mylog.txt

goto :eof
```

```
:cputime
set _pname=%1
set _pid=%2
set _t2=%8
set _t1=00:00:00

for /f "tokens=1 delims=" %%G in ('"find %1 p1.txt|find %2"') do (
   set _line=%%G
)

set _line1=%_line:,=%
set _line2=%_line1:"=,%
for /f "tokens=8 delims=," %%G in ("%_line2%") do (
   set _t1=%%G
)

for /f "tokens=1,2,3 delims=:" %%G in ("%_t1%") do (
   set _hh1=%%G
   set _mm1=%%H
   set _ss1=%%I
)

for /f "tokens=1,2,3 delims=:" %%G in (%_t2%) do (
   set _hh2=%%G
   set _mm2=%%H
   set _ss2=%%I
)

for /f "tokens=* delims=0" %%G in ("%_hh1%") do (set hh1=%%G)
for /f "tokens=* delims=0" %%G in ("%_hh2%") do (set hh2=%%G)
for /f "tokens=* delims=0" %%G in ("%_mm1%") do (set mm1=%%G)
for /f "tokens=* delims=0" %%G in ("%_mm2%") do (set mm2=%%G)
for /f "tokens=* delims=0" %%G in ("%_ss1%") do (set ss1=%%G)
for /f "tokens=* delims=0" %%G in ("%_ss2%") do (set ss2=%%G)

set /a _usage=((hh2-hh1)*3600+(mm2-mm1)*60+(ss2-ss1))*100/60

if %_usage% GTR %_maxusage% (
   if not %_pname%=="System Idle Process" (
      set _maxusage=%_usage%
      set _topname=%_pname%
      set _toppid=%_pid%
   )
)
```

SendEmail is a third-party command-line email client with TLS/SSL support, ver. 1.55, which can be downloaded from http://caspian.dotconf.net/menu/Software/SendEmail/.

References

Baker, E. T. Slade, R. M. Dorsey, M. E. Ruiz, L. M. and Duffin, G. L. 1986. Geohydrology of the Edwards aquifer in the Austin area, Texas: TWDB Rept. 293

Boy, J. P. Hinderer, J. and Gegout P., 1998. Global atmospheric loading and gravity, Physics of the planetary Interiors 109: 161-177

Chen, J.-L. Wilson, C. R. and Seo, K.-W. 2006. Optimized smoothing of Gravity Recovery and Climate Experiment (GRACE) time-variable gravity observations, J. Geophys. Res. 111 (B6)

Chapman, S. and Lindzen, R. S. 1970. Atmospheric tides: Thermal and gravitational, D. Reidel publishing company, Dordrecht, Holland

Crossley, D. Hinderer J. Casula, G. Francis O. Hsu, H.-T. Imanishi, Y. Jentzsch, G., Kääriänen, J. Merriam, J. Meurers, B. Neumeyer, J. Richter B. Sato, T. van Dam, T. 1999. Network of Superconducting gravimeters benefits a number of disciplines, E.O.S. 80 (11): 121-132

Crossley, D. Hinderer, J. and Rosat, S. 2002. Using atmospheric-Gravity Correlation to Derive a Time-Dependent Admittance Bull. Inform. Marees Terr. No. 136: 10809-10820

Dehant, V. Defraigne. P. and Wahr, J. M. 1999. Tides for a convective Earth, J. Geophys. Res. 104 (B1): 1035-1058

Farrel, W. E. 1972. Deformation of the Earth by surface load, Rev. Geophys. Space Phys. 10 (3): 761-797

Graham, S. T. Famiglietti, J. S. and Maidment, D. R. 1999. Five-Minute, 1/2º, and 1º Data Sets of Continental Watersheds and River Networks for Use in Regional and Global Hydrologic and Climate System Modeling Studies, Water Resources Research, 35 (2): 583-587

Han, S.-C. Shum, C.-K. and Braun, A. 2005a. High-resolution continental water storage recovery from low-low satellite-to-satellite tracking, J. Geodyn. 39 (1):11-28

Han, S.-C. Shum, C.-K. Jekeli, C., and Alsdorf, D. 2005b. Improved estimation of terrestrial water storage changes from GRACE, Geophys. Res. Lett. 32

Han, S.-C. Shum, C.-K., and Jekeli, C. 2006. Precise estimation of in situ geopotential differences from GRACE low-low satellite-to-satellite tracking and accelerometer data, J. Geophys. Res. 111 (B4)

Hunt B. B. Smith, S. Campbell, S. Liang. 2004, Groundwater-level monitoring program: example from the Barton Spring Segment of the Edwards aquifer, Central Texas. Texas Water Monitoring Congress.

Hutson, S. S. Barber, N. L. Kenny, J. F. Linsey, K. S. Lumia, D. S. and Maupin, M. A. 2004. Estimated use of water in the United States in 2000: Reston, Va., U.S. Geological Survey Circular 1268

Maclay, R. W. and Small, T. A. 1986. Carbonate geology and hydrology of the Edwards aquifer in the San Antonio area, Texas: TWDB Rept. 296

Neumeyer, J. Hagedoorn, J. Leitloff, J. and Schmidt, T. 2004. Gravity reduction with three-dimensional atmospheric pressure data for precise ground gravity measurements, J. Geodyn. 38: 437-450

Neumeyer, J. Barthelmes, F. Dierks, O. Flechtner, F. Harnisch, M. Harnisch, G. Hinderer, J. Imanishi, Y. Kroner, C. Meurers, B. Petrovic, S. Reigber, Ch. Schmit, R. Schwintzer, P. Sun, H.-P. and Virtanen, H. 2006. Combination of temporal gravity variations resulting from superconducting gravimeter (SG) recordings, GRACE satellite observations and global hydrology models, J. Geod., 79: 573-585

Prothero, W. A. and Goodkind, J. M. 1968. A Superconducting Gravimeter, Review of scientific instruments 39 (9): 1257 - 1262

Rodell, M. and Famiglietti, J.S. 2002. The potential for satellite-based monitoring of groundwater storage changes using GRACE: the High Plains aquifer, Central US, J. Hydrology. 263:245-256

Seo, K.-W. Wilson, C. R. Famiglietti, J. S. Chen, J.-L. and Rodell M. 2006. Terrestrial water mass load changes from Gravity Recovery and Climate Experiments (GRACE), Water Resou. Res. 42

Sharp, J., and Banner, J., 1997. Edwards Aquifer: a Resource in Conflict, GSA Today, vol.7 (8): 1-9.

Smith, A.B. Walker, J.P. Western, A.W. and Ellett, K.M. 2005. Using ground-based gravity measurements to monitor changes in terrestrial water storage, Engineers Australia 29th Hydrology and Water Resources Symposium, Canberra

Spratt, R. S. 1982. Modelling the effect of atmospheric pressire variations on gravity, Geophys. J. R. astro. Soc. 71: 173-186

Swenson, S. and Wahr, J. M. 2002. Methods for inferring regional surface-mass anomalies from Gravity Recovery and Climate Experiment (GRACE) measurements of time-variable gravity, J. Geophys. Res. 107 (B9)

Swenson, S. and Wahr, J.M. 2003. Estimated accuracies and regional water storage variations inferred from the Gravity Recovery and Climate Experiments (GRACE), Water Resou. Res. 39 (8)

Tapley, B.D. et. al. 2004. Grace measurements of mass variability in the Earth system, Science 305: 503-505

Van Camp, M. and Vauterin, P. 2005. Tsoft: graphical and interactive software for the analysis of time series and Earth tides, Computers & Geosciences, 31 (5): 631-640

Van Dam, T. M. and Wahr, J.M. 1987. Displacements of the Earth surface due to atmospheric loading: effects on gravity and baseline measurements, J. Geophy. Res. 92(B2): 1281-1296

Van Dam, T.M. and Francis, O. 1998. Two years of continuous measurements of tidal and nontidal variations of gravity in Boulder, Colorado, Geophys. Res. Lett. 25 (3): 393-396

Wahr, J.M. 1985. Deformation induced by polar motion, J. Geophy. Res. 90 (B11): 9363-9368

Wahr, J.M. and Molenaar, M. 1998. Time variability of Earth's gravity field" Hydrological and oceanic effects and their possible detection using GRACE, J. Geophys. Res. 103 (B12): 30,205-30,229

Wahr, J.M. Swenson, S. Zlotnicki, V. and Velicogna, I. 2004. Time-variables gravity from GRACE: First results, Geophy. Res. Lett. 31

Wahr, J.M. Swenson, S. and Velicogna, I. 2006. Accuracy of GRACE mass estimates, Grophy. Res. Lett., 33

Wenzel, H.G. 1996. The nanogal software: Earth tides data processing package: Eterna3.3 Bull. Inform. Marees Terr. No. 124, Obs. Royal de Belgique, Brussels, Belgium: 9425-9439

Wilson, C., Scanlon, B. Sharp, J., Longuevergne, L., Wu, H. 2011. Superconducting Gravimeter Observations of Water Storage Changes in the Edwards Aquifer, Groundwater Journal, submitted.